RADC-TR-81-116
Interim Report
June 1981

TENT SHAPED PHASED ARRAY

Harris Corporation

C. A. Chuang

ROME AIR DEVELOPMENT CENTER
Air Force Systems Command
Griffiss Air Force Base, New York 13441

This report has been reviewed by the RADC Public Affairs Office (PA) and is releasable to the National Technical Information Service (NTIS). At NTIS it will be releasable to the general public, including foreign nations.

RADC-TR-81-116 has been reviewed and is approved for publication.

APPROVED: John F McIlvenna

JOHN F. McILVENNA
Project Engineer

APPROVED: Allan C. Schell

ALLAN C. SCHELL
Chief, Electromagnetic Sciences Division

FOR THE COMMANDER: John P. Huss

JOHN P. HUSS
Acting Chief, Plans Office

If your address has changed or if you wish to be removed from the RADC mailing list, or if the addressee is no longer employed by your organization, please notify RADC (EEAA) Hanscom AFB MA 01731. This will assist us in maintaining a current mailing list.

Do not return this copy. Retain or destroy.

UNCLASSIFIED

SECURITY CLASSIFICATION OF THIS PAGE (When Data Entered)

REPORT DOCUMENTATION PAGE	READ INSTRUCTIONS BEFORE COMPLETING FORM
1. REPORT NUMBER: RADC-TR-81-116	2. GOVT ACCESSION NO.: AD-A103927	3. RECIPIENT'S CATALOG NUMBER
4. TITLE (and Subtitle): TENT SHAPED PHASED ARRAY	5. TYPE OF REPORT & PERIOD COVERED: Interim Report.
	6. PERFORMING ORG. REPORT NUMBER: N/A
7. AUTHOR(s): C. A. Chuang	8. CONTRACT OR GRANT NUMBER(s): F19628-79-C-0173
9. PERFORMING ORGANIZATION NAME AND ADDRESS: Harris Corporation, P.O. Box 37, Melbourne FL 32901	10. PROGRAM ELEMENT, PROJECT, TASK AREA & WORK UNIT NUMBERS: 62702F, 46001445
11. CONTROLLING OFFICE NAME AND ADDRESS: Deputy for Electronic Technology (RADC/EEAA), Hanscom AFB MA 01731	12. REPORT DATE: June 1981; 13. NUMBER OF PAGES: 72
14. MONITORING AGENCY NAME & ADDRESS (if different from Controlling Office): Same	15. SECURITY CLASS. (of this report): UNCLASSIFIED; 15a. DECLASSIFICATION/DOWNGRADING SCHEDULE: N/A

16. DISTRIBUTION STATEMENT (of this Report)

Approved for public release; distribution unlimited

17. DISTRIBUTION STATEMENT (of the abstract entered in Block 20, if different from Report)

Same

DTIC ELECTE SEP 9 1981 S D H

18. SUPPLEMENTARY NOTES

Project Engineer: John F. McIlvenna (EEAA)

19. KEY WORDS (Continue on reverse side if necessary and identify by block number)

Aircraft Arrays
Phased Arrays
Satellite Communications Antenna

20. ABSTRACT (Continue on reverse side if necessary and identify by block number)

This interim report presents the study results of a tent shaped phased array SHF aircraft antenna for Satellite Communications. The antenna consists of four planar phased arrays and has a low profile streamlined configuration. The tent array provides electrical scanning over a hemisphere and is capable of high power transmission. The design of the array is a trade-off of the key parameters including antenna coverage, gain, aerodynamic impact, high power transmission, and array packaging. → cont

DD FORM 1 JAN 73 1473 EDITION OF 1 NOV 65 IS OBSOLETE

UNCLASSIFIED

SECURITY CLASSIFICATION OF THIS PAGE (When Data Entered)

391655

cont.

The detailed design considerations of these parameters are presented. A design procedure is given to derive an optimum tent array configuration. The design of a 20 dB gain tent array is discussed. This array consists of square waveguide elements, septum polarizers, ferrite and diode phase shifters, a unique feed network, and a microprocessor for array control. The array depth has a significant impact on the aerodynamic effects and array packaging. The development and design of compact array components to reduce the array depth and to provide high power capability is the key factor to the successful application of the tent array. The extension of the 20 dB gain design to a 30 dB gain array is also included. A breadboard planar array, to test the performance of the array and components, and verify the concept of the tent shaped phased array, is being implemented in this effort.

TABLE OF CONTENTS

		Page
1.0	INTRODUCTION	1
2.0	ARRAY DESIGN CONSIDERATIONS	2
2.1	Key Array Design Parameters	2
2.2	Scan Contours	6
2.3	Array Configurations	10
2.4	Aerodynamic Impact	17
2.5	High Transmit Power	18
2.6	Array Packaging and Component Design	18
2.6.1	Antenna Element/Polarizer	18
2.6.2	Feed Network	24
2.7	Array Element Pattern	27
2.8	Mechanical Considerations	27
2.9	The Design of a 20dB Gain Tent Array	28
3.0	TENT SHAPED PHASED ARRAY	30
3.1	Tent Array and Square Waveguide Elements	30
3.2	Phase Shifters	34
3.3	Feed Network	34
3.4	Array Controller	41
3.5	Mechanical Structure	41
4.0	30DB GAIN ARRAYS	41
5.0	THE BREADBOARD ARRAY	46
6.0	CONCLUSION	48
	REFERENCES	50
	APPENDIX A	A-1
	APPENDIX B	B-1
	APPENDIX C	C-1

LIST OF FIGURES

		Page
Figure 1 -	Tent Shaped Phased Array Configuration	3
Figure 2 -	Airborne Antenna Configurations	4
Figure 3 -	Scan Contours (Side Array at 30°)	7
Figure 4 -	A Typical Scan Contour (End Array at 26°, Side Array at 34°)	8
Figure 5 -	Scan Contours (Side Array at 45°)	9
Figure 6 -	Array Configuration Design	11
Figure 7 -	Array Width and Number of Elements in Elevation Direction Versus Radome Height	12
Figure 8 -	Array Depth and Projected Area	16
Figure 9 -	Aerodynamic Study: Case 1 (A,B,C)	19
Figure 10 -	Aerodynamic Study: Case 1 (D,E,F)	20
Figure 11 -	Aerodynamic Study: Case 2 (A,B,C)	21
Figure 12 -	Aerodynamic Study: Case 3 (A,B)	22
Figure 13 -	Conceptual Feed Network	26
Figure 14 -	An Array and the Antenna Element	32
Figure 15 -	A Description of Septum Polarizer	33
Figure 16 -	Tent Array Phase Shifter Assembly	35
Figure 17 -	Tent Array Feed Network	36
Figure 18 -	Elevation Power Divider	38
Figure 19 -	E-Plane Power Divider	39
Figure 20 -	Azimuth Power Distribution	40
Figure 21 -	Tent Array Feed Network	42
Figure 22 -	Back View of the Tent Array Feed Network	43
Figure 23 -	Detailed Design of the Azimuth Power Divider	44
Figure 24 -	An Array Configuration	45
Figure A-1 -	Aircraft and Array Coordinates	A-2
Figure B-1 -	Stacked Unconventional Septums	B-2
Figure B-2 -	Cross Sections of the Unconventional Septum Polarizer Element	B-2
Figure C-1 -	Array and the Cylindrical Ground Plane	C-2
Figure C-2 -	Array Elements and Grids	C-2

LIST OF TABLES

		Page
Table 1 -	Tent Array Specifications	5
Table 2 -	Loss Budget	14
Table 3 -	Array Configuration and Element	15
Table 4 -	Summary of Air Drag Study	23
Table 5 -	The Design of a Typical 20dB Gain Tent Array	31
Table 6 -	The Design of a Typical 30dB Gain Tent Array	47

1.0 INTRODUCTION

There is interest in the design of an effective low profile, high gain, SHF aircraft antenna for Satellite Communications which provides coverage over the entire upper hemisphere. Existing SHF aircraft terminals use parabolic antennas enclosed in large radomes mounted at the top of the aircraft fuselage. The parabolic antenna represents the best developed and highest efficiency antenna design and provides the desired antenna gain over the coverage region. However, the excessive air drag produced by the large radomes makes this antenna configuration unattractive for many applications, especially for high performance aircraft. The design of a low profile SHF aircraft antenna to replace the parabolic antenna is a difficult and challenging problem.

Many attempts have been made to design low profile (flush-mounted or conformal) high gain aircraft antennas for this application. All of the array designs considered can be categorized into two basic approaches. One approach is to use two arrays to provide hemispherical coverage, one on each side of the airframe with beam overlap to assure adequate coverage at zenith. Another approach is to use a single array located at the top center of the fuselage to provide the hemispherical coverage. However, a single low profile antenna, such as a microstrip antenna array or an electro-mechanical steered phased array which scans the beam mechanically in azimuth and electronically in elevation[1], suffers severe gain degradation at low elevation scanning angles. These scanning losses are mainly due to geometrical and physical limitations[2] such as reflection, diffraction, aperture projection efficiency and polarization loss. Many of these losses are associated with the particular array ground plane of the aircraft fuselage. Surface wave techniques were successfully employed[2] to reduce the loss, but their applications are limited to less than 10 percent of the frequency bandwidth.

The approach of using two arrays offers a potentially realizable solution to the problem. However, the arrays still cannot provide efficient coverage near the nose and tail regions of the aircraft due to the same physical and geometrical limitations. Adequate coverage in these regions requires the array apertures to be far larger than that required

for other regions of coverage. Microstrip or stripline phased arrays are low-cost antenna candidates for this type of conformal aperture application. The use of diode phase shifters in these arrays limit their application in high power transmission because of the restricted power handling capabilities of the diodes.

This report presents a tent shaped phased array[3] consisting of four planar arrays arranged in a streamlined configuration and packed inside the tent structure as shown in Figure 1. The tent array is low profile and provides an electronically steerable beam for hemispherical coverage. The antenna is capable of high power transmission and provides an adequate gain coverage near the horizon. It is a compromise solution between gain coverage and aerodynamic impact. A descriptive comparison of the antennas is given in Figure 2.

In the following, the array design considerations such as gain, hemispherical coverage, aerodynamics, transmitting power, array packaging, and their effects on the design of array components are presented. A detailed design and implementation of a 20dB gain tent array is given. The extension of the design to a 30dB gain array is dicussed. A breadboard array will be constructed in the remaining program period to demonstrate the performance and to verify the concept of the tent shaped phased array.

2.0 ARRAY DESIGN CONSIDERATIONS

A study was performed to design a tent shaped phased array to meet the antenna specifications shown in Table 1. The design of an optimum array configuration and the selection of array components depend on the effective trade-offs among the design parameters. A detailed consideration of these parameters is given in the following.

2.1 Key Array Design Parameters. The antenna specifications given in Table 1 include transmit and receive operation, dual circular polarization, 20dB gain for near hemispherical coverage, -20dB sidelobes in the azimuth plane, high transmit power (3KW), and physical constraints. The design of array components to meet the antenna performance requirements is complicated by the interactions of these parameters.

TENT SHAPED PHASED ARRAY CONFIGURATION

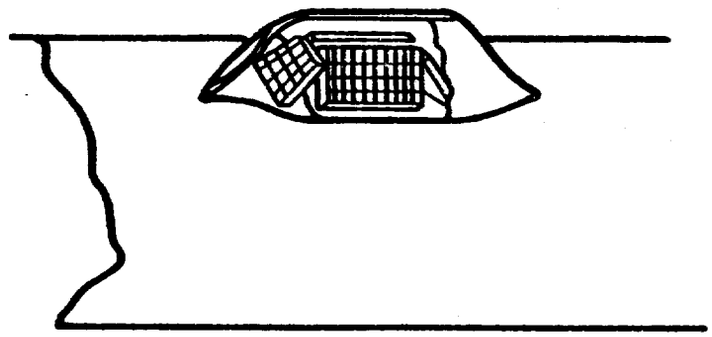

11738-2

FIGURE 1

AIRBORNE ANTENNA CONFIGURATIONS

LOW PROFILE FLAT ARRAY (ELECTRONIC SCANNING)

- MINIMUM AIR DRAG
- UNSATISFACTORY GAIN NEAR HORIZON

TENT ARRAY (ELECTRONIC SCANNING)

- LOW AIR DRAG
- SATISFACTORY GAIN

REFLECTOR (MECHANICAL SCANNING)

- HIGHER AIR DRAG
- DESIRED COVERAGE GAIN

FIGURE 2

11738-3

TABLE 1. TENT ARRAY SPECIFICATIONS

Frequency:	7.25 to 7.75 GHz, receive 7.90 to 8.4 GHz, transmit
Polarization:	RHCP, transmit LHCP, receive
Axial Ratio:	3 dB to within 10^{o} of horizon
Gain:	20 dB except 30^{o} half cone at nose and tail where 18 dB is acceptable.
Sidelobes:	-20 dB in the azimuth plane -12 dB in the elevation plane
VSWR:	< 2:1
Power:	3 kW CW, goal
Physical Requirements:	- Maximum tent size: 36" length, 8" height - Conform to C-135 type aircraft - 5" radius maximum aircraft hole

An essential requirement is adequate coverage over the hemispherical region such that a satisfactory communication link with the satellite can be maintained. The gain requirement is a prime factor in determining the size and shape of the antenna, which in turn controls the aerodynamic drag of the antenna. Since the antenna consists of four planar arrays arranged in a tent shaped configuration, the coverage of each array can be traded off and the array configuration can be optimized to minimize the aerodynamic impact and to provide the maximum gain coverage over the hemispherical region. The antenna components such as the aperture elements, polarizers, phase shifters, and feeding network must be designed not only to meet the requirements of frequency, polarization, gain, and sidelobes, but also to be capable of handling high transmit power and satisying the size constaints of the tent shaped configuration. The optimum array configuration is basically a trade-off among coverage gain, aerodynamics, and the mechanical structure needed for array packaging. The high power requirement has direct impact in the design of array components.

2.2 Scan Contours. Figures 3, 4, and 5 show the scan contours for two arrays mounted in the tent shape in which the end array has 3dB less gain than the side array. The scan contours[3] are scanning gain contours of a side array and an end array plotted on a half of the top hemisphere of the aircraft. The coordinates of such a scan contour plot are aircraft coordinates, i.e., azimuth and elevation angles. A zero azimuth angle represents the aircraft nose direction. A zero elevation angle is the aircraft vertical axis. The coordinates are obtained by transforming the constant gain contours of the arrays from local coordinates to the aircraft coordinates. The gain values in the scan contours are the peak obtainable gains for an array beam scanned to the indicated directions. The equations of coordinates transformation can be found in Appendix A.

The scan contour is a useful tool in determining an optimum array configuration for the desired coverage. By assuming the scan contours at -3.5dB to be the maximum allowable scanning loss, the shaded areas of the scan contours represent the regions where the gain specification cannot be met. For given end and side arrays, the shaded area can be minimize by properly tilting the arrays to form an optimum tent configuration. In Figure 3, the side array is tilted at 30° and the tilt angle of the end

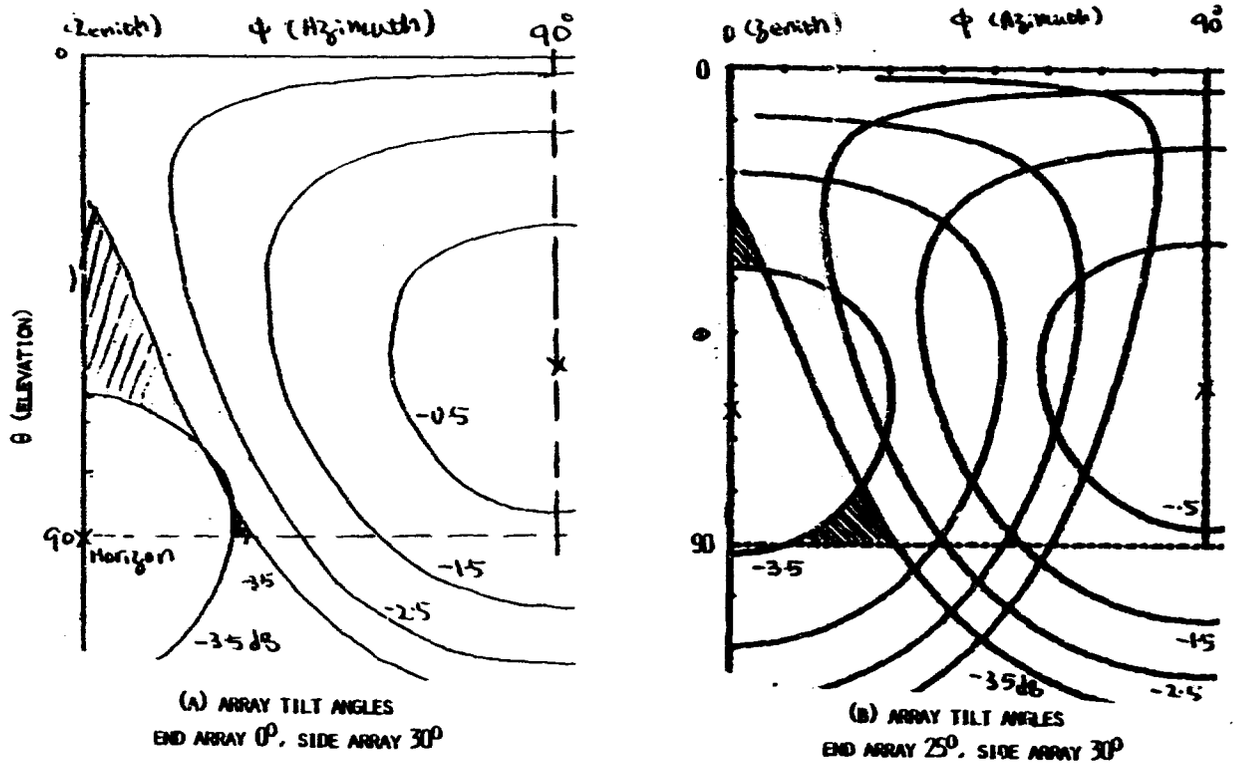

(a) ARRAY TILT ANGLES
END ARRAY 0°, SIDE ARRAY 30°

(b) ARRAY TILT ANGLES
END ARRAY 25°, SIDE ARRAY 30°

FIGURE 3 SCAN CONTOURS (SIDE ARRAY AT 30°)

A TYPICAL SCAN CONTOUR
(END ARRAY AT 26°, SIDE ARRAY AT 34°)

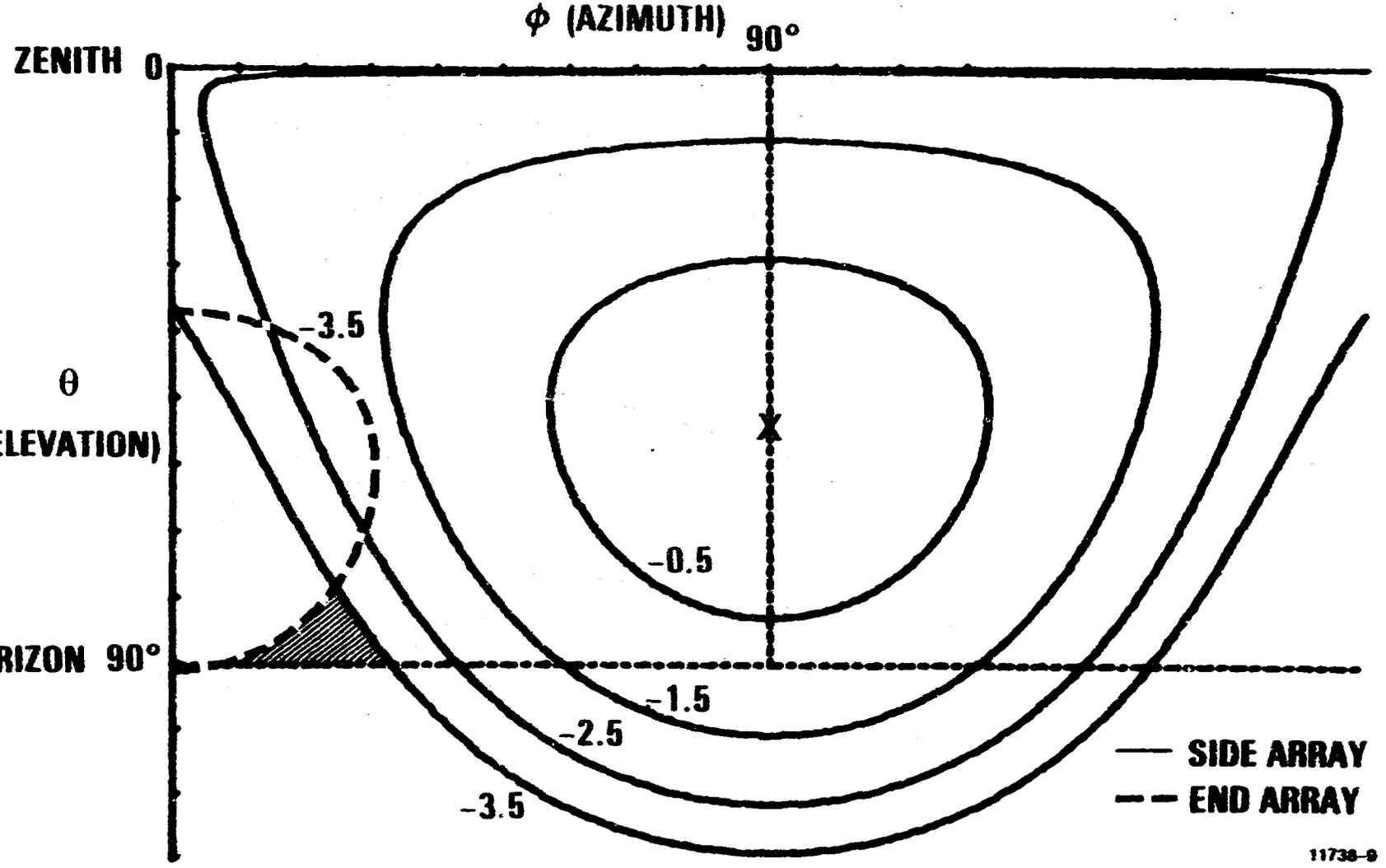

FIGURE 4

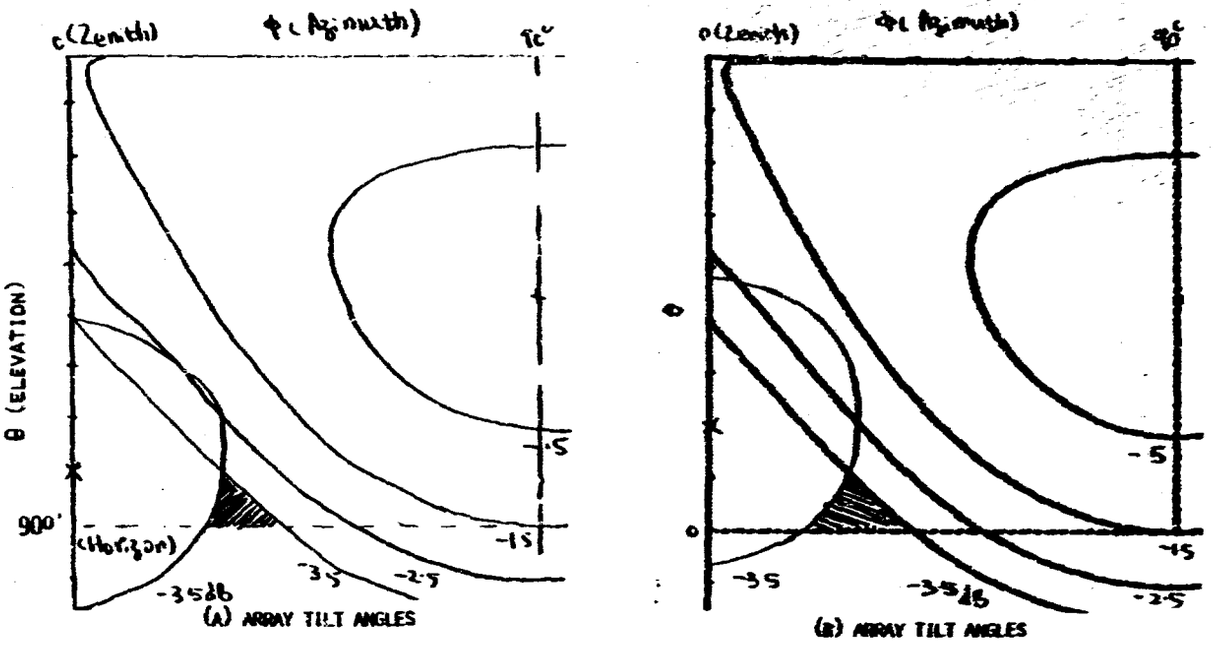

FIGURE 5 SCAN CONTOURS (SIDE ARRAY AT 45°)

array is varied to minimize the shaded area. Figure 4 presents the optimum array configuration for the case where the tilt angles of the side arrays are 34^{o}. Figure 5 shows the contours with side arrays tilted at 45^{o}. A study of the scan contours reveals that the configuration with side arrays tilted at 45^{o} and front array at 10^{o} represents a nearly optimum solution of the coverage problem. It was also observed that small variations in tilt angle from the "optimum" solution do not significantly degrade the performance. Hence the tilt angles of the array can be approximately chosen for the convenience of aerodynamic concern and the mechanical packaging of the array.

2.3 Array Configurations. The array configuration design process is shown in Figure 6. The design parameters which significantly impact the array configuration and packaging are the scan contour, radome height, and the array depth. For a given gain requirement, the scan contours are used to obtain values of scan angles and tilt angles for each of the end and side arrays as discussed in Paragraph 2.2. The maximum scan angles determine the maximum array spacings that can be used without introducing grating lobes. The array components including the antenna element apertures, polarizers, phase shifters, and the feed network set the array depth and the array loss. The total array aperture is calculated from the required gain, scan loss at maximum scan angle, and the array loss. The tilt angle and the maximum allowable radome height limit the array height. Then, the remaining dimensions of the array and also of the radome are calculated from the required array aperture. If the resulting array configuration is aerodynamically acceptable, the array configuration is frozen. Otherwise, the design process is iterated by varying the scan contour, radome height, and array depth.

Figure 7 shows the array dimensions of an array design as a function of the radome heights. In this array design, the tilt angles of side array and end array are 45^{o} and 20^{o} respectively from the vertical positions. The maximum scanning angle is 63^{o} for the side array, and 30^{o} for the end array. The depth of the arrays is fixed at 10 inches for dielectric loaded waveguides and 11.5 inches for no dielectric loaded waveguides. The required array aperture is calculated using an array loss of 4.23dB (without

ARRAY CONFIGURATION DESIGN

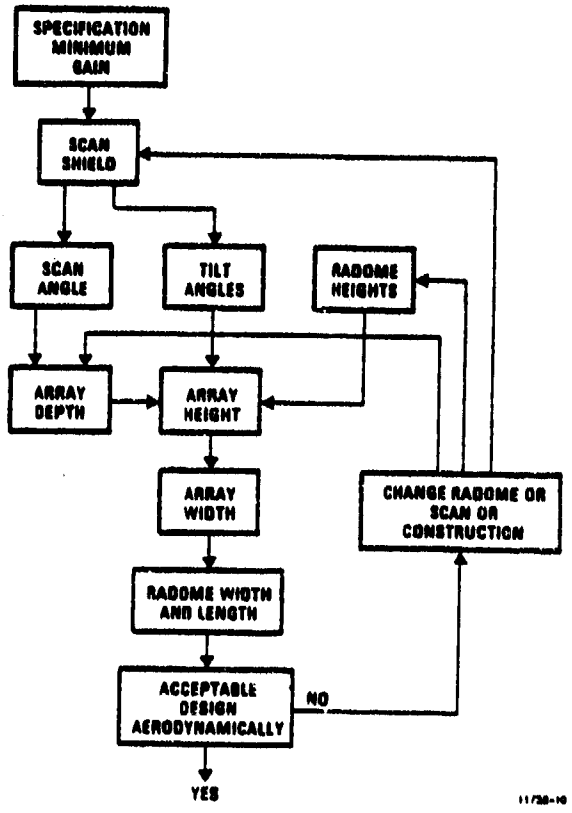

FIGURE 6

FIGURE 7. ARRAY WIDTH AND NUMBER OF ELEMENTS IN ELEVATION DIRECTION VERSUS RADOME HEIGHT

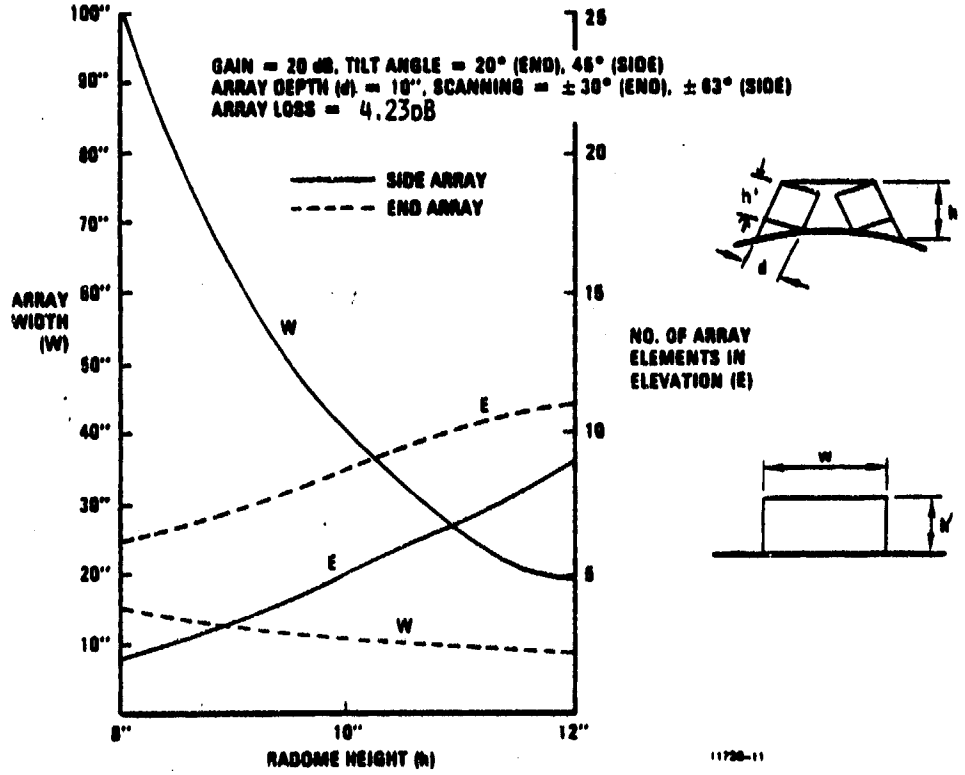

counting the scan loss). It is shown in Figure 7 that at a radome height of 8 inches, the side array width is 100 inches, which results in disproportionately large side arrays and far exceeds the required tent configuration of 36 inches. A compromise between the radome height and length must be made. The loss budget of the arrays is shown in Table 2. The detailed computation of the array dimensions is presented in Table 3. An active element pattern loss of IdB was used for ground plane effects, in addition to the aperture projection factor.

The depth of the array has a direct impact on the array configuration design. If the array depth is less than 10 inches as shown in the above example, more array elements can be placed in the vertical direction for a given radome height and the problem of required array width can be alleviated. The array depth depends on the dimensions of the selected array components such as the element apertures, polarizers, phase shifters, and the feed network. The minimum array depth is limited by the achievable array component dimensions which must be designed to meet the array requirements of operating frequencies, scanning, polarization, and high power capacity. The minimum array depth, and thus the array packaging configuration, is directly proportional to the efforts taken for the development of array components.

The array depth also has a significant aerodynamic impact on the array projected area in the streamline direction. The projected array areas of the array configuration given in Figure 7 are plotted in Figure 8 as functions of the array depth. The projected areas are normalized to the array area with zero thickness. The radome height is fixed at 8 inches. The larger projected area of the end and side arrays is the projected area of the tent array configuration. It is interesting to note that the side array dominates the projected area until the array depth reaches approximately 9 inches. It should be noted that this relationship of projected area is a function of the antenna gain and the tilt angles of the arrays. The projected area of the end array will play a more important role when the required antenna gain is increased or the tilt angle of the end array is reduced. The importance of the array depth in the design of array configuration is significantly reduced when the required antenna gain is increased to 30dB.

TABLE 2

LOSS BUDGET

	Side Array (63^{o} Scan)	End Array (30^{o} Scan)
Scan Loss	3.5dB	0.5dB
Phase Shifter	1.0	1.0
Phase Quantization	0.5	0.5
Polarizer	.05	.05
Aperture Active Impedance	1.25	1.25
Radome	.3	.3
Waveguide Feed Network	1.0	1.0
Polarization Mismatch	.13	.13
TOTAL	7.73dB	4.73dB

TABLE 3 ARRAY CONFIGURATION AND ELEMENT

	SIDE ARRAY			END ARRAY (DIELECTRIC LOADED)			END ARRAY (NO DIELECTRIC LOADING)		
Scan Sector	$\pm 63^{\circ}$			$\pm 30^{\circ}$			$\pm 30^{\circ}$		
Tilt Angle	45°			20°			20°		
Minimum Gain (dB)	20			20			20		
Total Losses (dB)	7.73			4.73			4.73		
Directivity (dB)	27.73			24.73			24.73		
Aperture Size (in^2)	157.4			78.9			78.9		
Element Spacing (in)	.79			.78			.933		
Array Depth - d (in)	10			10			11.5		
RADOME HEIGHT - h (IN)	8	10	12	8	10	12	8	10	12
Array Height - h' (in)	1.56	3.9	7.02	4.68	7.02	8.58	3.73	6.53	8.40
Array Width - w (in)	101.4	40.56	22.62	17.16	11.7	9.36	21.46	12.13	9.33
Array Elements	2 x 130	5 x 52	9 x 29	6 x 22	9 x 15	11 x 12	4 x 23	7 x 13	9 x 10
Number of Elements	260	260	261	132	135	132	92	91	90

ARRAY DEPTH AND PROJECTED AREA

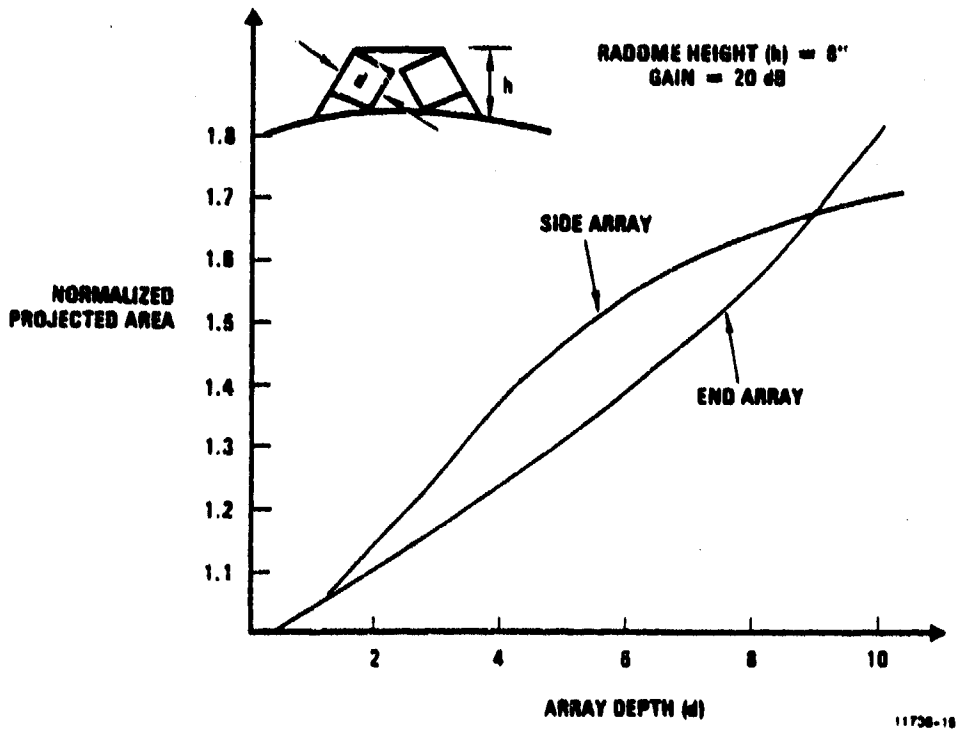

FIGURE 8

2.4 Aerodynamic Impact. Any protrusion on the aircraft body will result in some drag increase which ultimately manifests itself in a reduction in speed and range of the aircraft. The tent array will be enclosed in a streamlined radome in the shape of a half body. The shape, that is, its length (l) to height (h) ratio has been selected to minimize the local drag coefficient C_{do}. The theory of fluid dynamic drag[4] indicates that the l/h ratio must be at least 10-12 in order to minimize the drag coefficient and consequently the drag. The width of the half body and its trailing edge must also be the optimum dynamic shape. For a least drag design, the radome has to be of considerable length, consequently the trailing edge is not a desirable RF window because of the long acute angles of the sandwich shell.

An approximate estimate of the value of drag caused by the radome is given by:

$$\text{Drag} = C_{do} \times S \times q$$

Where C_{do} = Local drag coefficient
S = project area in ft^2
q = dynamic pressure ($lbs./ft^2$)

and dynamic pressure is given by:

$$q = 1/2\rho V^2$$

Where V = m.p.h.
and $1/2\rho$ is a constant which is a function of air density.

For example, for an aircraft flying at 600 m.p.h. at 35,000 ft

$$q = 0.00095 \times 600^2$$
$$= 341 \text{ lbs./ft}^2$$

Selecting a radome with a projected area (head-on into the wind) of 2.5 ft^2 and of sufficient streamlining (l/h approx. 10), $C_{do} = 0.045$.

Thus drag = $0.045 \times 2.5 \times 341$
= 38.4 lbs.

This is a near optimum shape of the radome. However, it is not best suited as an RF window, consequently a compromise has to be made which will increase the drag.

Figures 9-12 presents a variety of radome shapes for enclosing the tent array configurations. A summary of the estimated radome weight and the potential increase in fuel consumption for these array and radome configurations is shown in Table 4. The 20dB gain tent array design described in Figure 7 and a cylinder shape similar to the C-135 aircraft fuselage, were used for estimating the radome weight and the fuel consumption percentage for this particular requirement. Every attempt should be made to reduce the overall array projected area.

2.5 High Transmit Power. The high transmit power requirement impacts the array component designs in several ways. It definitely influences the choice of phase shifters and their design, and necessitates that at least a portion of the feed network be waveguide. The compact packaging required for aerodynamic considerations and close element spacing may lead to thermal problems under high power operation. The power consideration suggests that the array component designs be waveguide structures.

2.6 Array Packaging and Component Design. The tent arrays must be packed into the tent configuration to minimize the aerodynamic drag. The array package has been identified as a major issue and has a great impact on the design of array components such as antenna aperture, polarizer, phase shifter, and feed network. As discussed in Section 2.5, the high transmit power requirement dictates the use of ferrite phase shifters for transmit, and waveguide type structures for antenna elements and feed network, which in turn, imposes a severe packaging problem for the array. The design considerations of antenna element, polarizer, and feed network are discussed in the following.

2.6.1 Antenna Element/Polarizer. The considerations of high power transmission and dual circular polarization operation suggest the use of an integral element of square waveguide and a septum polarizer[5]. Although the septum polarizer has a drawback of a relatively long dimension from launching point to aperture, its selection was based on the following:

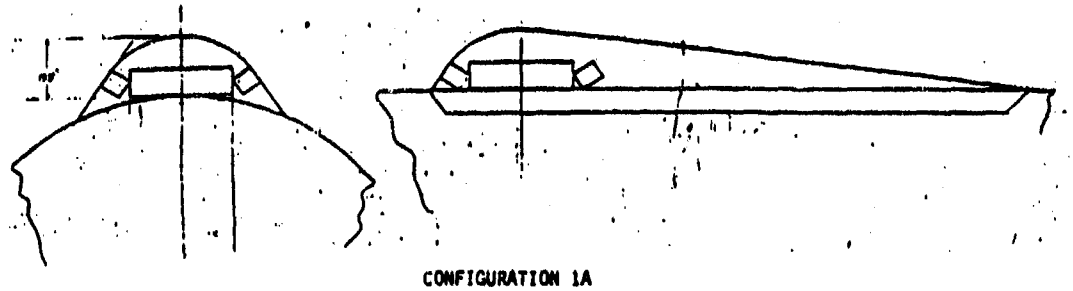

CONFIGURATION 1A

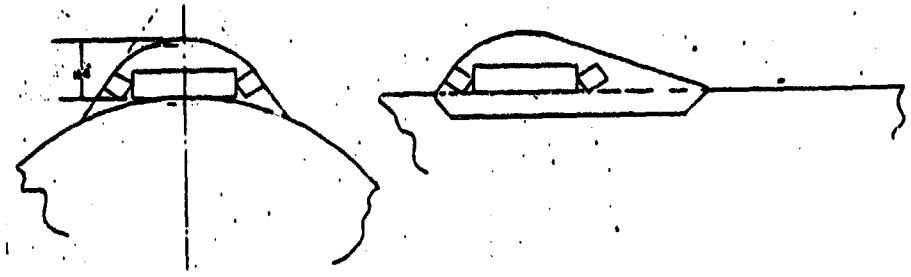

CONFIGURATION 1B

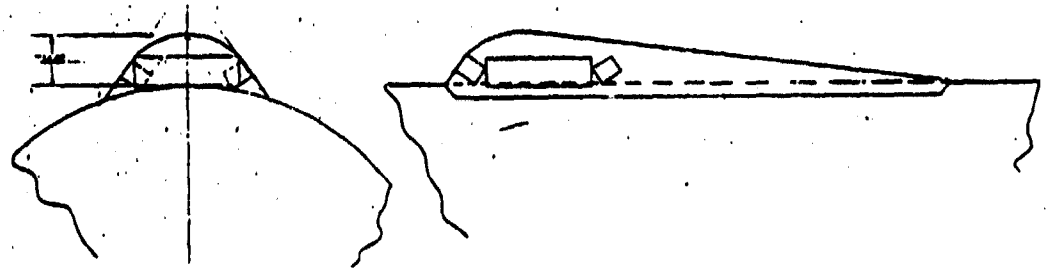

CONFIGURATION 1C

FIGURE 9 AERODYNAMIC STUDY: CASE 1 (A,B,C)

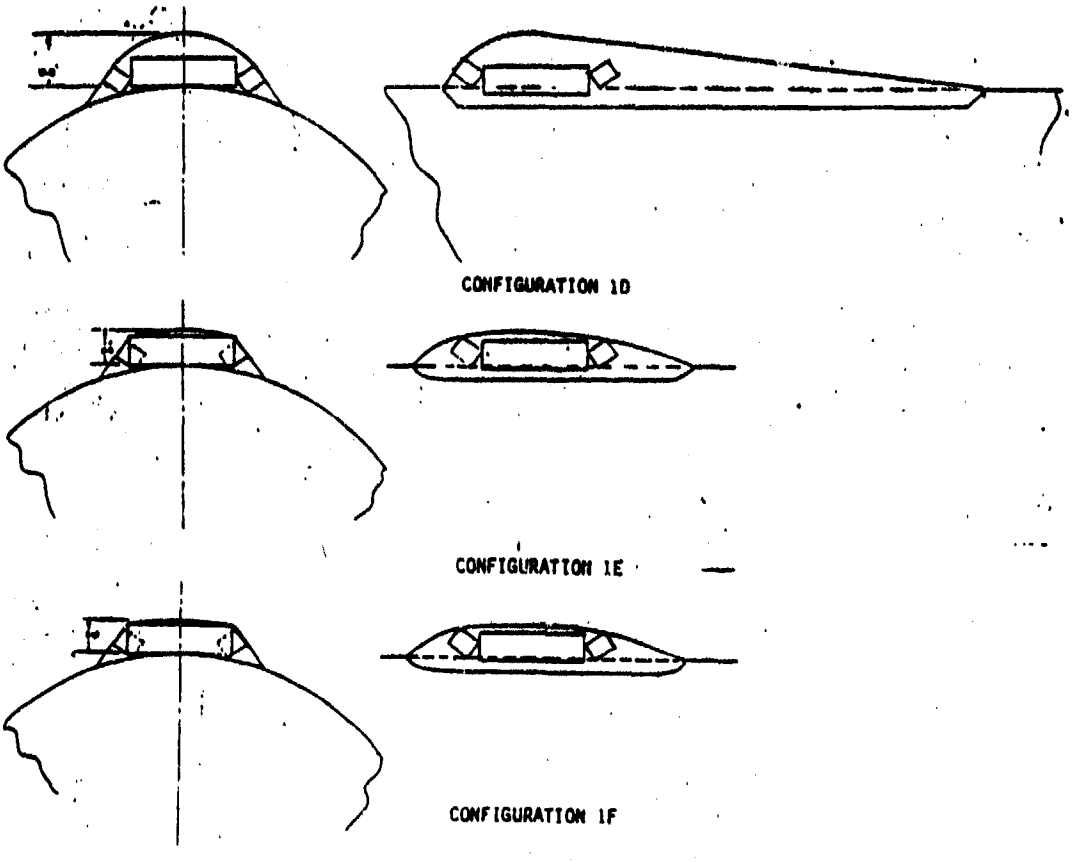

FIGURE 10 AERODYNAMIC STUDY: CASE 1 (D,E,F)

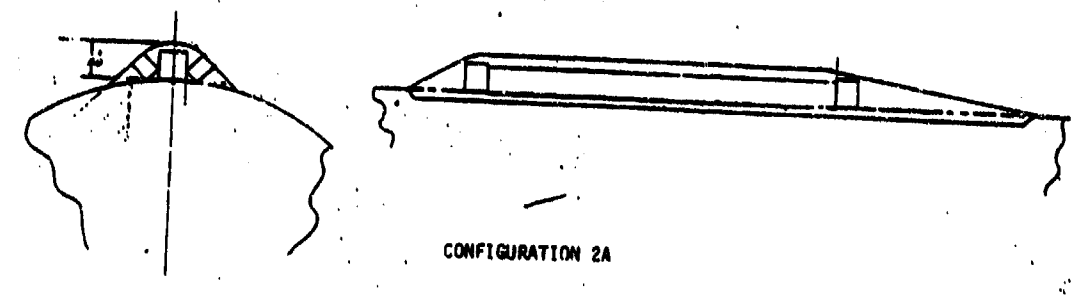

CONFIGURATION 2A

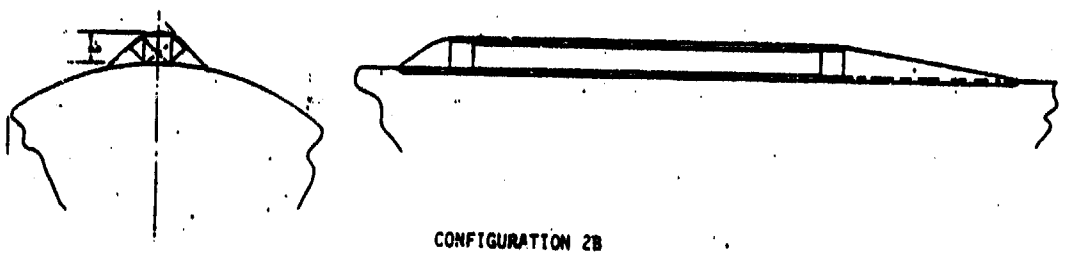

CONFIGURATION 2B

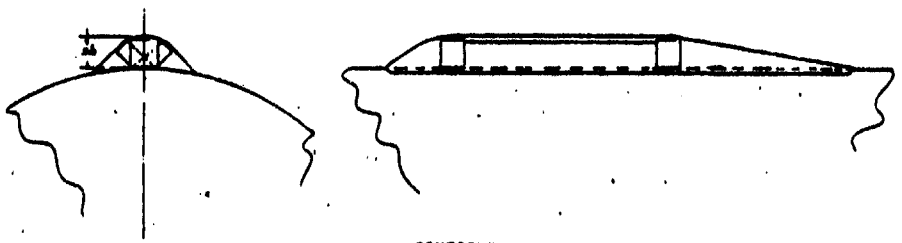

CONFIGURATION 2C

FIGURE 11 AERODYNAMIC STUDY: CASE 2

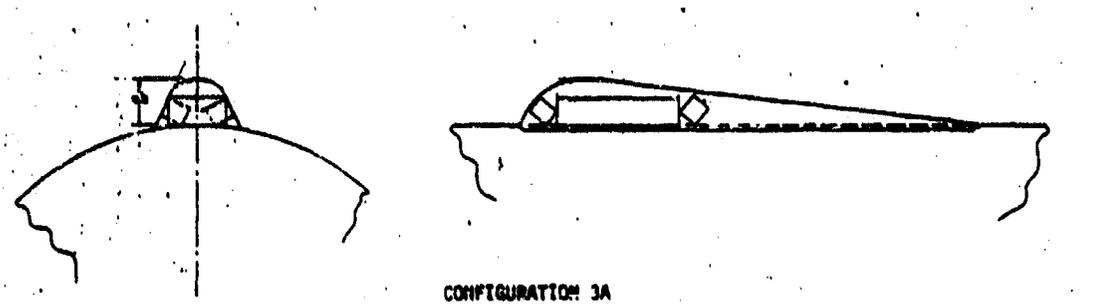

CONFIGURATION 3A

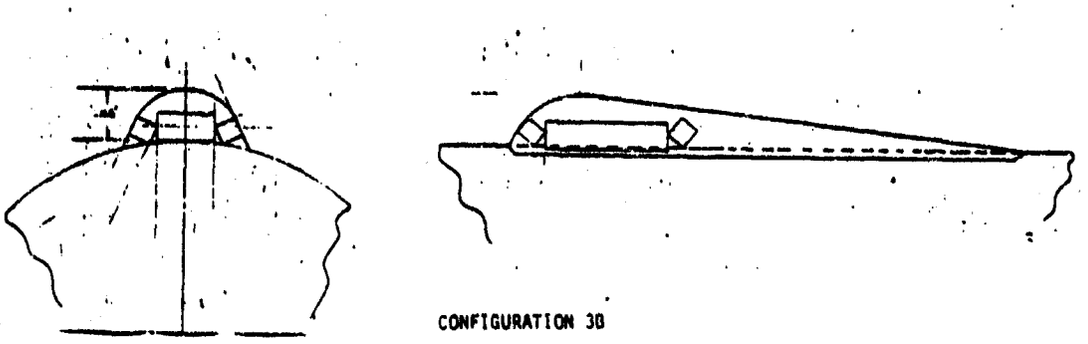

CONFIGURATION 3B

FIGURE 12 AERODYNAMIC STUDY: CASE 3

CONFIGURATIONS		S(FT^2)	C_{DO}	S × C_{DO}	EST WEIGHT (LBS)	INCREASE IN FUEL CONSUMPTION(%)
1	A	5.2	0.03	0.155	68	0.43
	B	5.165	0.05	0.258	34.5	0.72
	C	3.42	0.03	0.103	50	0.29
	D	4.305	0.035	0.15	60	0.42
	E	2.44	0.04	0.098	26.5	0.27
	F	2.3	0.045	0.103	27.5	0.29
2	A	1.7	0.065	0.1105	48	0.30
	B	1.15	0.065	0.074	38	0.22
	C	1.15	0.055	0.063	28	0.18
3	A	2.86	0.035	0.100	40	0.28
	B	1.67	0.03	0.050	29	0.15

11738-14

TABLE 4. SUMMARY OF AIR DRAG STUDY

1) The compact in-line geometry of this type of polarizer has a high packing factor.

2) The dual orthogonal circularly polarized outputs eliminate the need for a diplexer and allow one antenna element to be used for both the transmit and receive functions.

3) All waveguide structure minimizes the RF loss.

4) It accepts relative high power.

5) It has good on-axis ratio and good polarization isolation.

6) Its simple mechanical configuration permits repeatable and low cost production units.

The basic tent array design requires the side array to be capable of scanning to $\pm 60^{o}$. The array element spacing must be small enough to prevent the generation of grating lobes at a frequency of 8.4GHz when the beam is scanned to the extreme angle. However, this type of element spacing will make the element below cut-off at a frequency of 7.25GHz. One method of overcoming the problem is to load the waveguide and feed assembly completely with dielectric material. Other alternative methods include the use of ridge waveguide and the use of an unconventional septum polarizer. The ridge waveguide approach requires the utilization of triangular ridges to reduce the possibility of generating unwanted TE_{21} modes at the waveguide and septum transition. The concept of an unconventional septum polarizer involves the use of a nonuniform rectangular waveguide in the septum region such that the dielectric loading or ridges can be eliminated. A description of such an unconventional septum polarizer is presented in Appendix B. Although the latter two methods offer potential solutions to the problem, the practical application of these techniques cannot be achieved without further study. Thus, dielectric loading is recommended.

2.6.2 Feed Network. The major considerations dominating the feed network design include the power handling capability, low loss, and

compactness. The feed network is intimately associated with the array size and hence the aerodynamic impact on the aircraft. A low loss feed network is essential to minimize the aperture size. A waveguide feed is in general low loss and thus is desirable for this application. The compact packaging of a waveguide feed behind the array aperture requires an innovative electrical and mechanical design. The aperture elements will be closely spaced to avoid grating lobes at large scan angles, consequently, a waveguide feed network may have to be dielectrically loaded to physically fit the available space behind the aperture. The problems of interaction between the power taps, and controlling the amplitude to each of the aperture elements, given the size constraints, requires new accuracy. Impedance matching is an important requirement for the feed network design. A nonbinary type of feeding structure is appealing because of the requirement for compactness. Phase compensation methods must also be considered for phased array operations.

One conceptual design of a nonconventional feed network is illustrated in Figure 13. As is shown in the figure, the matrix of aperture elements is connected directly to the polarizing section. The two waveguide outputs of the polarizers connect to separate transmit and receive phase shifters. These phase shifters are in turn connected to the narrow wall of a common waveguide through a controlled coupling hole or slot. The common guide has the same height dimension as the phase shifters and polarizer output. The broad dimension of the common guide is adjusted to provide one guide wavelength spacing between the coupling apertures to provide controlled coupling to all of the elements in each row. This common guide is fed from a T junction at the center of the array. After a right angle H plane, bend the common guides from rows of elements are combined to a single transmitter port. A similar arrangement can be used for the receive function with the combiner located on the opposite side of the centerline of the array. This feed configuration provides a very compact low loss waveguide system for both the receive and transmit modes. The amplitude taper required for the -20dB sidelobe level can be obtained through the properly controlled waveguide coupling of the elements. However, the mutual coupling among the amplitude coupling holes in the common waveguide presents amplitude and

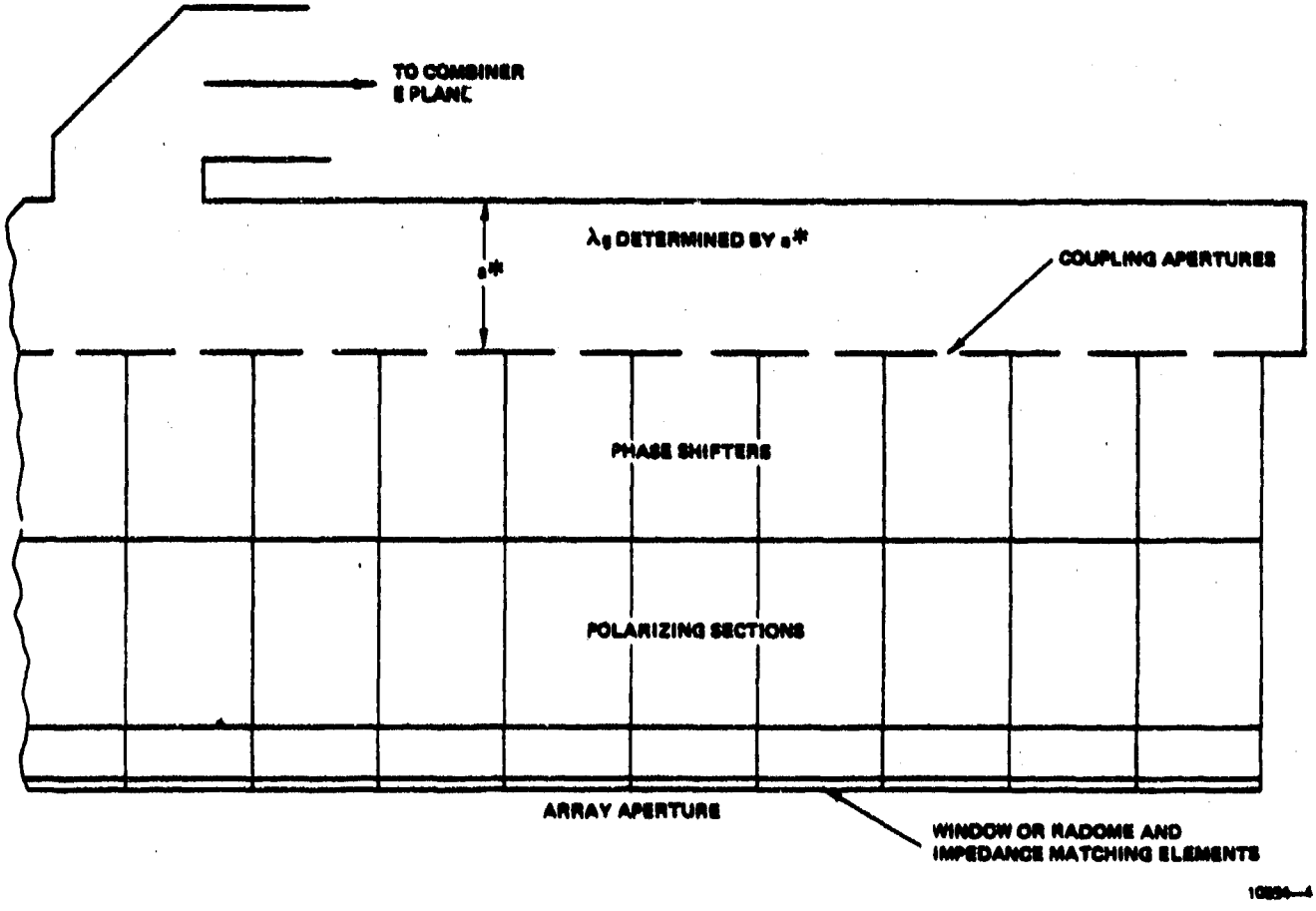

FIGURE 13 CONCEPTUAL FEED NETWORK

phase errors. Impedance matching for the entire frequency band requires special treatment. An alternate design of the feed network is to use septum type power dividers for proper power distribution and amplitude tapering, and to use step transformers for impedance matching. The latter feed network increases the array depth slightly compared to the former one, but eliminates the problem of mutual coupling. The selection between the two is a trade-off of development effort and array depth. A detailed description of this latter feed network will be presented in Section 3.

2.7 Array Element Pattern. The actual array radiation pattern must be used in the study of scan contours and array coverage. The array pattern can be obtained by computing the array active element patterns including the array mutual coupling and finite array edge effects. The effects of the cylindrical ground plane on the active elements may be estimated by using the theory of geometrical optics. The array pattern is then computed as the summation of the products of the array factor and the element patterns. A simple method of computing the element pattern is given in Appendix C.

2.8 Mechanical Considerations. Since the tent array is intended for airborne use, light weight is a main consideration. It is therefore important that each element of the array be as light as practical, hence thin wall techniques must be employed. The elements would be individually constructed with thin walls and bonded into an array. This is a two-fold attack to minimize cost. It reduces the risk of an array being unusable because of a flaw in one or two elements, and leads to a repetitive production of identical parts. Very thin wall investment casting, as is frequently used in airborne and spaceborne electronics boxes, would lend itself well to these requirements.

There are high vibration levels in aircraft as well as some shock. Regardless of the importance of light weight, the assembled array must be capable of withstanding the vibration, operational shock, and crash safety shock. The array must be tightly packaged in order to meet the electrical performance requirements. Each element must be assembled directly in contact with its neighbors, consequently access to and room for mechanical fasteners is unavailable. Should it be structurally necessary, casting can

be produced in brazeable alloys so that the array could be dip brazed. Adhesive bonding of the elements is most attractive. It provides sound structural integrity and low temperature cures, avoiding warping. Further, it permits handling and adjusting in low cost tooling during assembly.

Access to the interior of the aircraft must also be made available. By mounting the array control unit on top of the aircraft between the array faces, only two waveguides and a power supply cable will penetrate the skin. These can be arranged to require an access hole less than 3 inches in diameter. It is desirable to make this access pressure tight to maintain the interior aircraft pressure and to prevent the radome from experiencing a pressure differential. A fiberglass reinforced plastic (FRP) can be used for the radome and must be relatively thin wall to minimize the electrical effects. The radome can incorporate a fairing for aerodynamic efficiency. The fairing may cause electrical distortion, but the distortions can be preprogrammed into the controller after testing. Local reinforcing of the radome is required where the radome attaches to the aircraft to withstand the forces of high speed flight and the vibration and shock. Consistently similar FRP radomes are possible using wet layup and vacuum bag techniques with a precision mold.

2.9 The Design of a 20dB Gain Tent Array. The dominating factors of design parameters and considerations presented in previous paragraphs are antenna gain for hemispherical coverage, the physical constaints for aerodynamic performance, and the high power radiation. The gain coverage over a hemisphere is a prime factor in determining the required aperture size and shape of each of the four planar arrays. The size and shape of the tent array controls the aerodynamic impacts of the antenna. The high transmit power consideration suggests that the array component designs be waveguide structures, which in turn impacts the array packaging and aerodynamic effects. The design of an optimum tent array is basically a trade-off of gain coverage, aerodynamics, and mechanical structure of the array components for packaging.

The study of array coverage using scan contours indicates that the

array configuration with side arrays tilted at 45^{0} and front end arrays at 10^{0} represents a nearly optimum solution of the coverage problem. It was observed that small variation in tilt angle from the "optimum" solution do not significantly affect the array performance. Thus, the end and front arrays can be tilted at a large angle, such as 20^{0}, to provide better coverage in regions other than horizon.

The study of aerodynamic impact concluded that the array projected area plays a more important role than the radome streamline shape in the increase of fuel consumption percentage for the tent array requirements. The array configuration, the radome height, and the component dimension must be designed to reduce the overall array projection area.

A block diagram was presented in Figure 6 to illustrate the iterative array design procedure. The most significant design parameters are the radome height and array depth. They interact with each other and have direct impact on the array packaging and aerodynamic effects. As is shown in Figure 7 and Table 3, if the radome height is fixed at 8 inches and array depth at 10 inches, the required array width of the side array is approximately 100 inches, which is much longer than the desired length of 36 inches. This array length can be reduced to a reasonable size by using more compact array components or increasing the height of the overall array. The maximum allowable height of the array is mainly specified in the concern of the aerodynamic impact. The minimum array depth is limited by the achievable array component design, which must be designed to meet the requirements of operating frequencies, scanning, and high power capability. An array depth of 10 inches is achievable using existing hardware of square waveguides, septum polarizer, and the step transformer type of power combiner. The use of a nonconventional power combiner (Figure 13) and a compact septum polarizer and phase shifter is capable of reducing the array depth to 6 inches. The minimum obtainable array depth is then proportional to the effort taken for the development of compact array components.

The various array dimensions given in Table 3 were calculated based on the array losses of 7.73dB for the side arrays, and 4.73dB for the end and front arrays. The array loss can be minimized and the array aperture

size reduced by carefully matching the array aperture and controlling the mutual coupling effects.

A typical 20dB tent array designed to best meet the array specifications is presented in Table 5. This array employs the array configuration with side arrays tilted at 45^{o} and end arrays at 20^{o} to provide optimum gain coverage. The array losses of 6.98dB and 3.98dB are used for the side and end arrays. The element spacing of .78 inches is designed for the side arrays in the consideration of grating lobes at maximum scanning angle. The same element spacing is used for the end arrays in the concern of mechanical fabrication and array packaging. The array depth of 6 inches is assumed based on the use of an unconventional power combiner and a compact septum polarizer and phase shifter. The array has the overall array size of a height of 8 inches and a length of 38 inches. The total required number of array elements is 524.

3.0 TENT SHAPED PHASED ARRAY

The design implementation of the tent shaped phased array consisting of four planar phased arrays is presented in this section. Each face of the array consists of square waveguide elements, septum polarizers, ferrite phase shifters for transmit and diode phase shifters for receive, and a compact feed network. The step transformer type of feed network is used, which results in an array depth of 10 inches. A microprocessor provides the functions of beam steering and phasing correction. A detailed description of the components is given in the following.

3.1 Tent Array and Square Waveguide Elements. One planar array of the tent shaped arrays with 8 x 12 elements is shown in Figure 14 for the purpose of illustration. The array consists of 96 square waveguide element modules, compactly packed and fed by a low loss feed network. The element module contains the open-ended square waveguide aperture, a septum polarizer, and phase shifters for transmit and receive. The element module is dielectric loaded to eliminate grating lobes. The septum polarizer is considered as an integral part of the antenna element. It is selected for the dual polarization operation of the tent array. The cross section views of the septum polarizer as shown in Figure 15 demonstrates the technique of generating

TABLE 5. THE DESIGN OF A TYPICAL 20DB GAIN TENT ARRAY

	Side Array	End Array	Total Array
Scan Sector	$\pm 63^{o}$	$\pm 30^{o}$	-
Tilt Angle	45^{o}	20^{o}	-
Minimum Coverage Gain (dB)	20	20	20
Total Losses (dB)	6.98	3.98	-
Directivity (dB)	26.98	23.98	-
Required Aperture Size (in^2)	105	52.6	-
Element Spacing (in)	.78	.78	.78
Array Depth - d* (in)	6	6	-
Array Height - h'* (in)	4.68	6.24	-
Array Width - W* (in)	22.62	8.56	-
Array Elements	6 x 29	8 x 11	-
Number of Elements	174	88	524
Overall Array Size:			
Height - H* (in)	8	8	8
Length - (in)	-	-	38
Radome Configuration			1E**

*The symbols of the array dimensions are illustrated in Figure 7.

**See Figure 10.

AN ARRAY AND THE ANTENNA ELEMENT

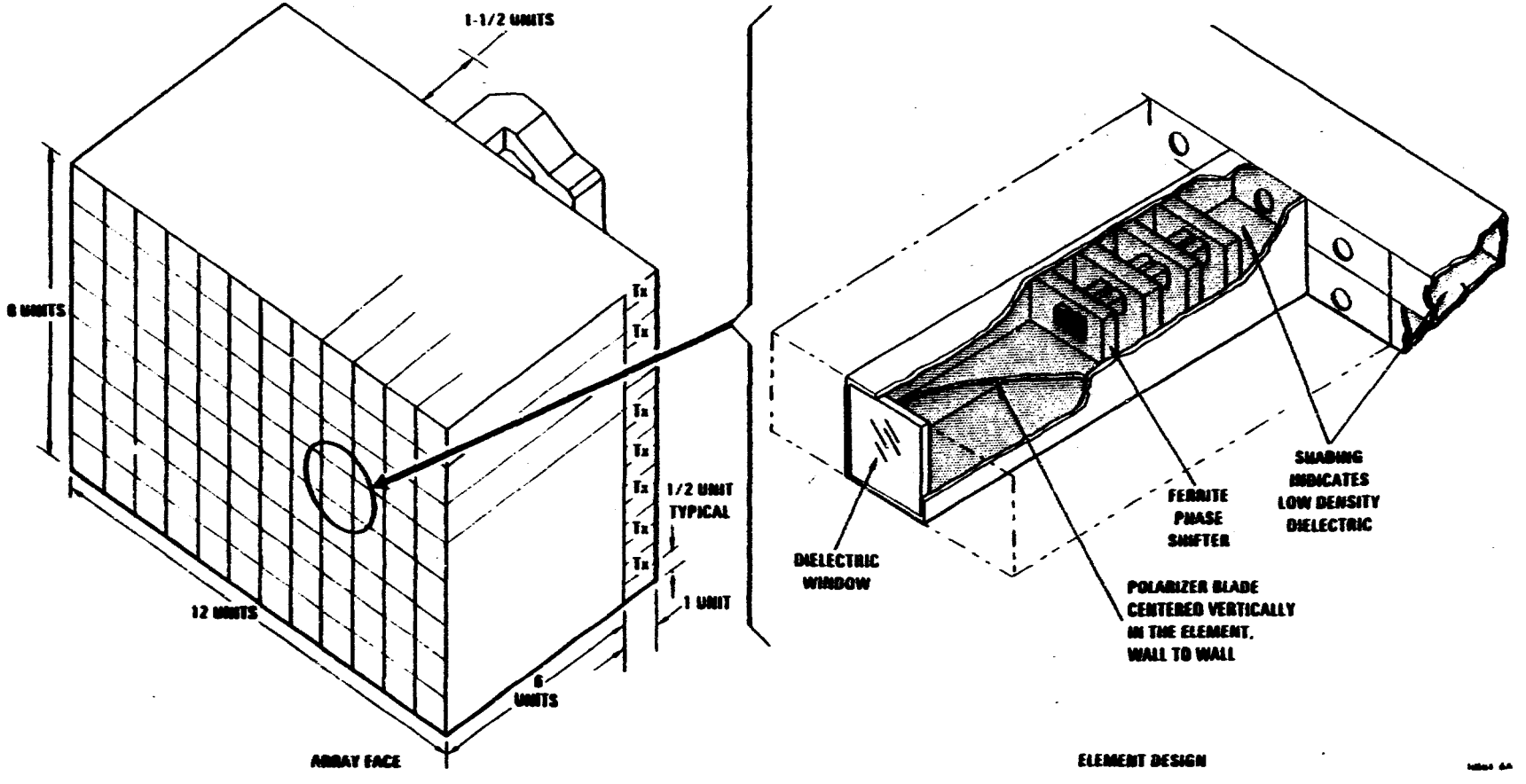

FIGURE 14

A DESCRIPTION OF

SEPTUM POLARIZER

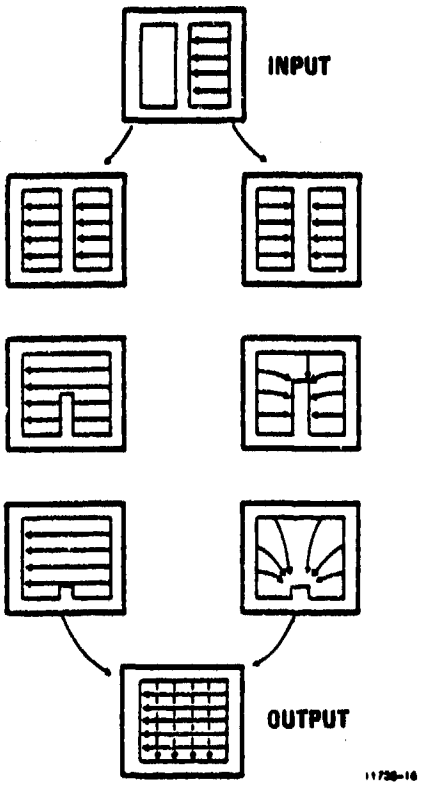

FIGURE 15

circularly polarized signals through the septum transformation. It should be noted that the array elements in Figure 14 are configured in a square grid. In practical applications, the elements can be arranged in a triangular grid which offers a potential reduction in the number of antenna elements needed[6]. In addition, the triangularly packaged array has a positive effect on the axial ratio performance of the array pattern.

3.2 Phase Shifters. For the tent array application, ferrite phase shifters are selected for the transmit operation, and 4-bit diode phase shifters are recommended for receive. Diode phase shifters have higher insertion loss and lower power capability, but have advantages of size, weight, and cost. The ferrite phase shifters have the disadvantages of size and weight. The use of ferrite phase shifters in transmit ports of tent arrays is necessary for high power operation. The selection of diode phase shifter for receive is mainly in the consideration of weight and cost. A 4-bit diode phase shifter is preferred for the tent array due to the concern of sidelobe level generated by the phase quantization error.

The physical layout and dimensions of the phase shifters in the waveguide system are shown in Figure 16. The ferrite phase shifter requires a driver card which contains logic and analog circuitry. This circuitry is hybridized and mounted in the receive side of the waveguide system along with the receive diode phase shifter, as shown in Figure 16. The receive phase shifter is a microstrip hybrid-coupled bit circuit, and is matched to the waveguide on both ends with coupling probes. It requires no drive card or separate power lines. Eight control lines are required for each element. The control circuit wires must run outside the waveguide corners because of the array element spacing and the location of the phase shifters, hence each element in the array is chamfered, forming a channel sufficient to permit the wires to pass.

3.3 Feed Network. A complete feed network was designed for the 12 element wide by 8 element high array. The network provides amplitude tapering in the azimuth plane for 20dB sidelobe levels and provides uniform amplitude in the elevation plane. A section of the feed network connecting to three rows of element modules is shown in Figure 17. The feed network

TENT ARRAY PHASE SHIFTER ASSEMBLY

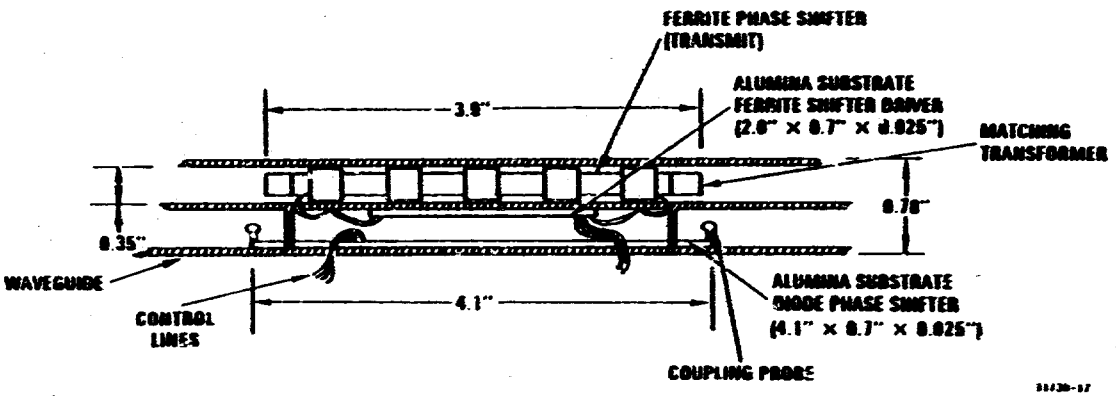

FIGURE 16

TENT ARRAY

FEED NETWORK

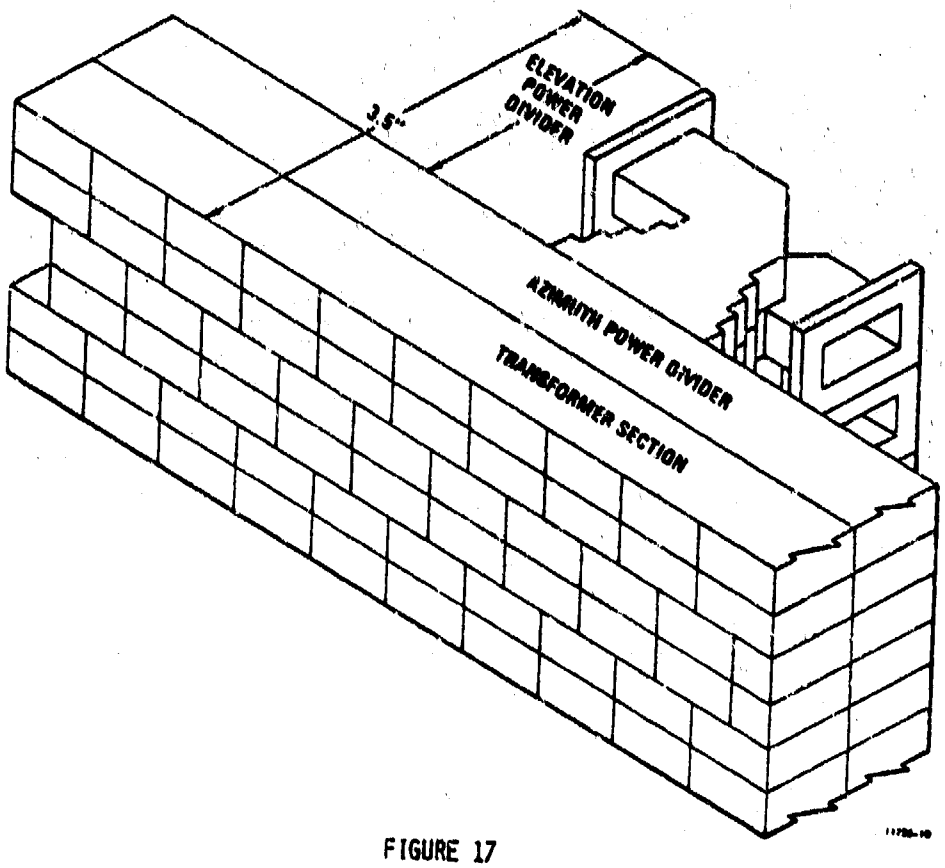

FIGURE 17

is conveniently described in the terminology of transmit. As is shown, the feed network consists of three major parts; namely, the elevation power divider, the azimuth power divider, and the waveguide transformer.

The elevation power divider consists of two E-plane binary power dividers, one for transmit and one for receive, and the associated H-plane tees. The binary power dividers that connect to the flanges of the H-plane tees are not shown in Figure 17. The H-plane tees feed the 12:1 azimuth power dividers which divide the power into the 12 elements with proper amplitude taper. The transformer section converts the odd size coupling hole in the azimuth power divider to the standard size guides of the element modules.

The H-plane tee feeding the center of the 12:1 power divider is folded as shown in (1), (2), and (3) of Figure 18. There are two, 12:1 power dividers which are mounted back to back for transmit and receive. These 12:1 power dividers are fed by a pair of H-plane tees, back to back, as shown in (4) of Figure 18.

Each 12:1 azimuth power divider consists of two identical (but mirror image) 6:1 power dividers fed at the center by the H-plane tee. The 6:1 power dividers splits the waveguide in the E-plane in the ratio of the desired power. For instance in Figure 19, if one-third of the available power is to be split off the main line, a septum dividing the guide in the E-plane into 1/3 and 2/3 will split the power 1/3 and 2/3 at the junction. The third of the power split off can then be routed to an antenna element and the remaining power can then be further divided by other antenna elements further down the array. In the figure the waveguide which was 2/3 height waveguide is then stepped up to full size for the next power split. This is not absolutely necessary if the septums are infinitely thin or the number of elements are few, but for six elements some increase in guide height is deemed necessary after each division.

A section of the waveguide at the center of the azimuth power divider is shown in Figure 20. Two array elements located at the center of the waveguide are directly fed by the input step transformer through the thin septum in the upper wall of the azimuth power divider. The remaining electrical powers are guided by the septums in the waveguide divider to feed

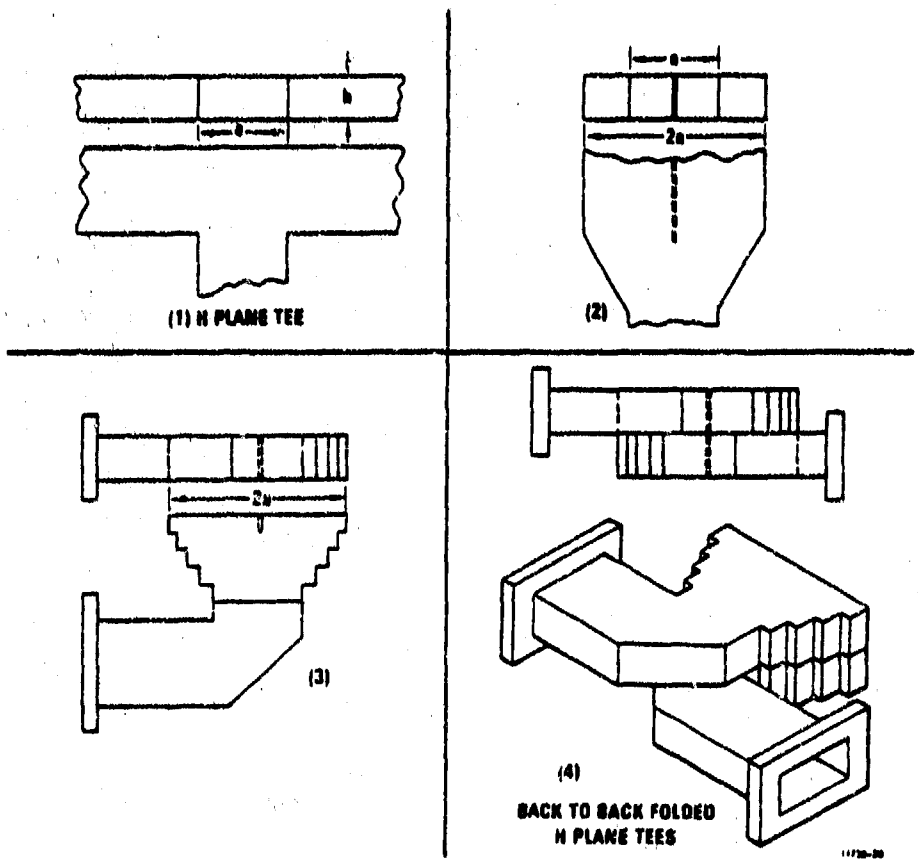
ELEVATION POWER DIVIDER
(1) H PLANE TEE
(2)
(3)
(4)
BACK TO BACK FOLDED
H PLANE TEES

FIGURE 18

E PLANE POWER DIVIDER

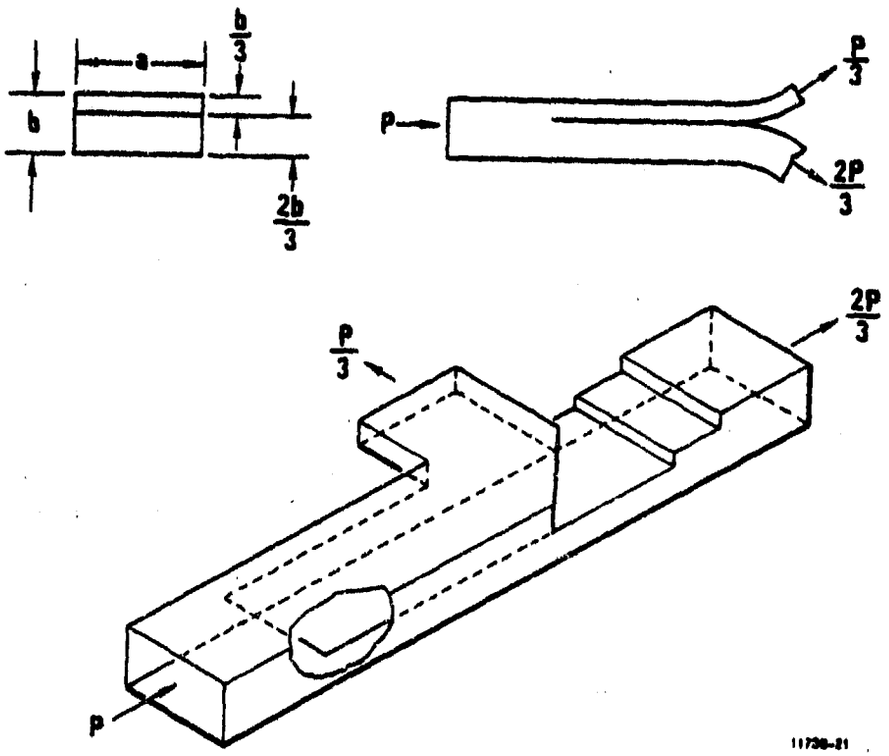

FIGURE 19

AZIMUTH POWER DISTRIBUTION

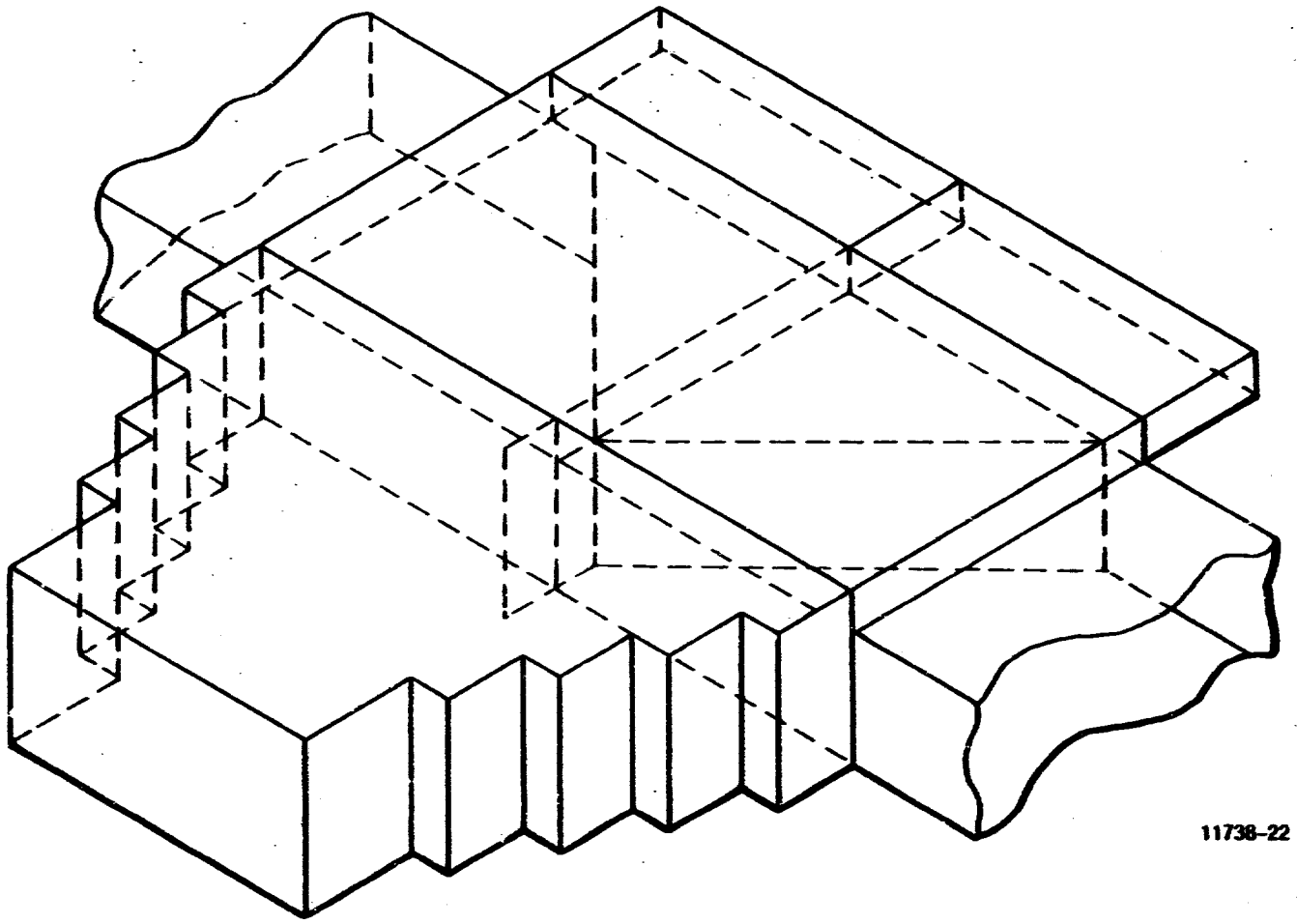

FIGURE 20

the rest of the elements. The cross section view of the half of the azimuth power divider and elements fed are shown in Figure 21. The design detail of the azimuth power divider for feeding the waveguides to provide a -20dB sidelobe is given in Figure 22. A back view of the entire array showing the transmit and receiving ports is presented in Figure 23.

3.4 Array Controller. A microprocessor is suitable to perform the array controller functions of the tent array. The microprocessor accepts beam pointing and frequency commands inputs, and provides control signals to the array phase shifters. The control signals are generated by the processor through the performance of many functions including array aperture switching logic, coordinate transformation, feeding phase error correction in frequency, and calculation of phase shift based on scan angle, frequency and element positions. A microprocessor type of array controller is also capable of performing additional functions such as beam search and automatic calibration.

3.5 Mechanical Structure. An array configuration for the tent array is shown in Figure 24. Thin wall techniques are used to make the elements of the array as light as practical. The array is also tightly packed and fastened to meet electrical performance and to withstand vibration and shock. Access to the interior of the aircraft is made available by mounting the array controller unit on top of the aircraft between the array faces. Since only two waveguides and a power supply cable will penetrate the aircraft skin, an access hole of less than 3 inches in diameter is required.

4.0 30DB GAIN ARRAYS

The design considerations and procedure presented in Section 2.0 are directly applicable to the design of a 30dB gain antenna. The antenna configuration will be similar to the one used for the 20dB gain antenna. The major difference between the design of a 20dB gain antenna and a 30dB gain is the impact of the element depth. For a 20dB gain antenna, the achievable component depth limits the array packaging configuration and has a significant aerodynamic impact on the array projected area in the streamline direction. For a 30dB gain antenna, the effects of component depth on the aerodynamic impact is greatly reduced because in this case the

TENT ARRAY FEED NETWORK

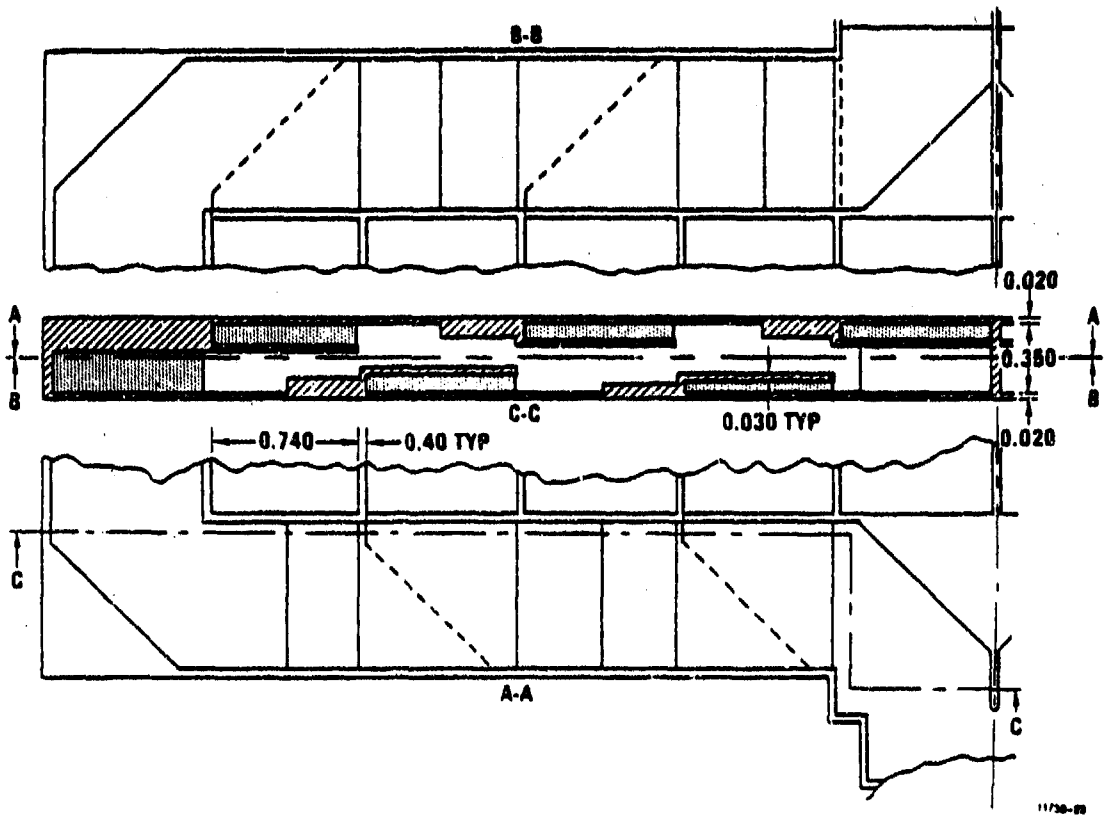

FIGURE 21

BACK VIEW OF THE

TENT ARRAY FEED NETWORK

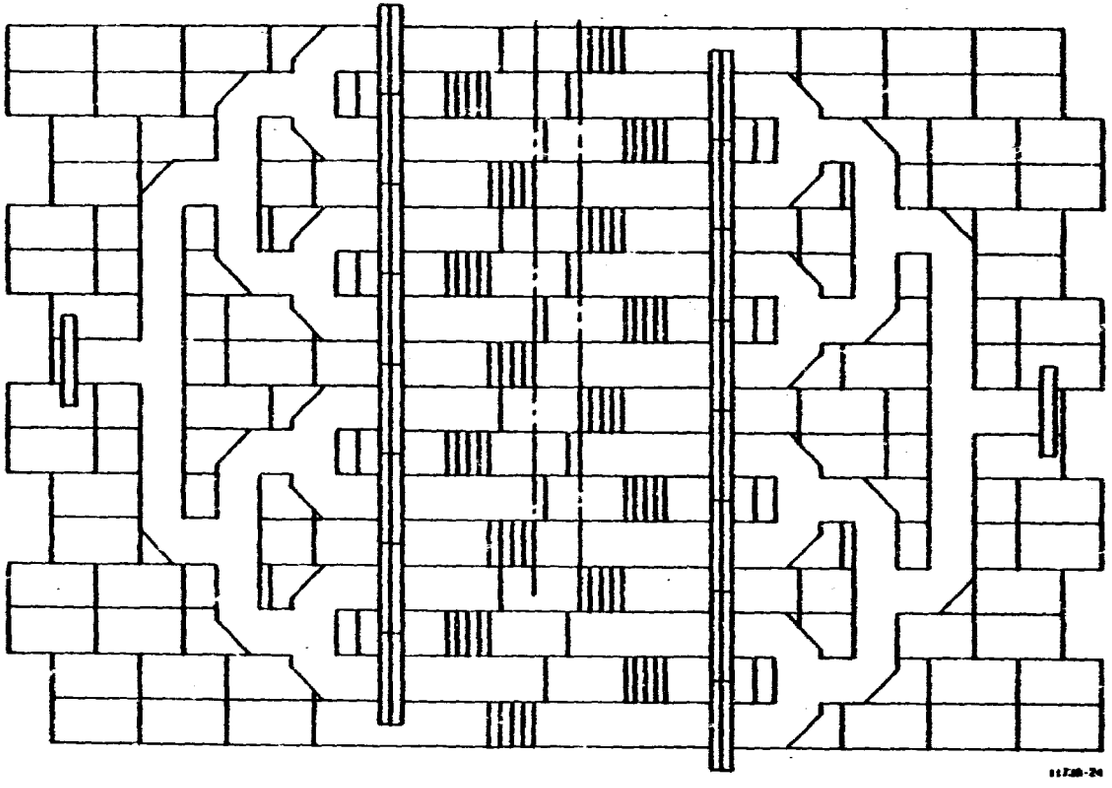

FIGURE 22

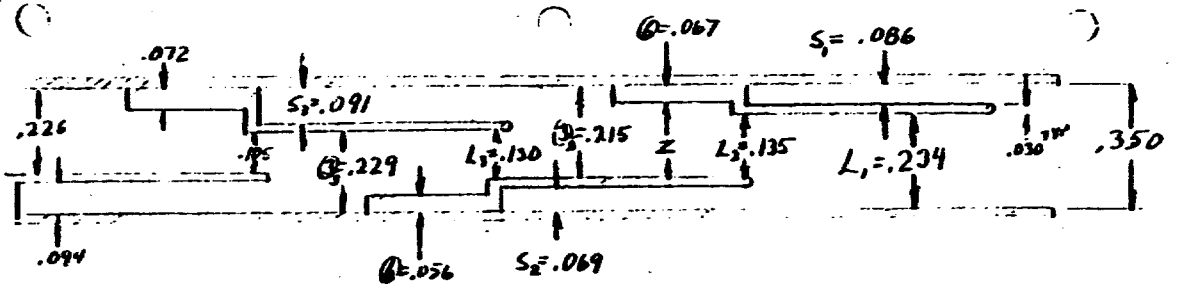

① = S_1 = (③$_{i-1}$ - .030) x $\frac{ZP_1}{100}$ ② = L_1 = (③$_{i-1}$ - .030) x $\frac{ZP_1}{100}$ FOR S_1 & L_1, ③$_4$ = .350

# FROM E	TAPER IN DB	TAPER IN POWER	POWER AVAIL.	% POWER USED	% POWER LEFT	(1) S_1	(2) L_1	(3) .32-S	(4) R=③/②	(5) Z(②x⑤)	(6) STEP ③-⑤
1	0	1	3.74	27	73	.086	.234	.234	-	-	-
2	.3	.93	2.74	34	66	.069	.135	.215	1.86	.184	.067
3	1.3	.74	1.81	41	59	.091	.130	.229	1.76	.173	.056
4	3.0	.50	1.07	47	53	.094	.105	.226	2.15	.154	.072
5	5.0	.32	.57	56	44	.110	.086	.210	2.44	.134	.076
6	6.0	.25	.25	100	0	.210	0	-	-	-	-

FIGURE 23 DETAILED DESIGN OF THE AZIMUTH POWER DIVIDER

AN ARRAY CONFIGURATION

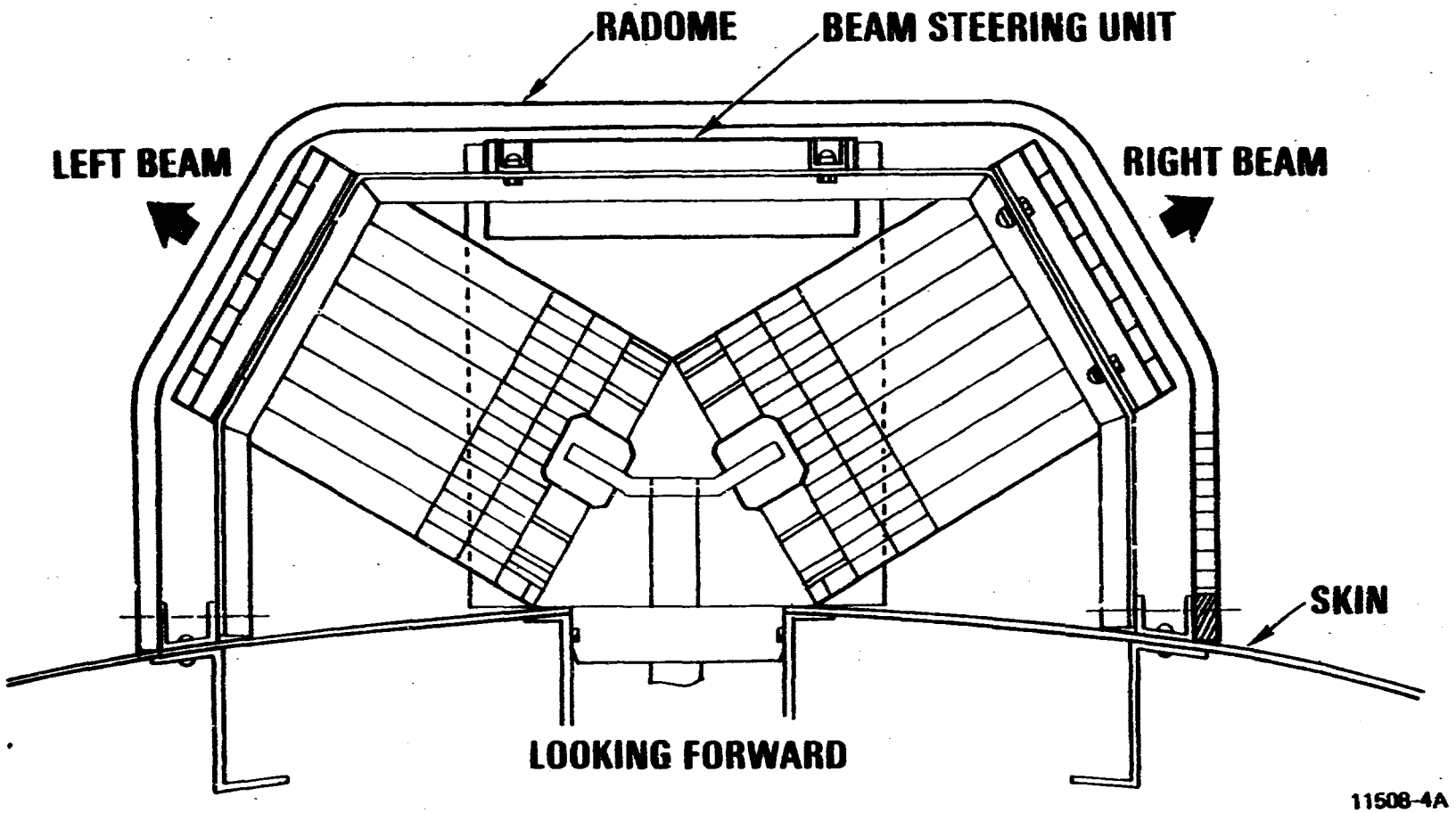

FIGURE 24

antenna aperture of the end array dominates the projected area in the streamline direction.

The design of a typical 30dB gain tent array is given in Table 6. For the purpose of comparison and illustration, this array employs the same array tilt angles, maximum scan angles, and array depth as the ones used for the 20dB gain antenna presented in Table 5. The total array loss was increased by .2dB for the additional loss in the waveguide combiner. The overall array height has been increased to 12 inches as a trade-off of the array dimensions for a reasonable tent array length in the streamline direction and an adequate array width acrossing the fuselage cross section. The overall array length is 119 inches. Since the impact of the array depth to the packaging is reduced, large waveguides with no dielectric loading are used for the end arrays. The total required number of array elements is 4,888.

The 30dB gain array in Table 6 illustrates the extension from the 20dB design to the one of 30dB. The required larger antenna aperture increases the aerodynamic impact of the aircraft. The array configuration must be optimized through many design iterations. For instance, in the case of 20dB gain antenna, it may not be advantageous to tilt the end array away from the vertical position due to the constaint of component depth and its effects on the array packaging. For a 30dB gain antenna, it appears to be more desirable to tilt the end array as far as allowable such that the end arrays can be used to cover more of the scan region and consequently, the scanning requirements of the side arrays can be reduced. In addition, the designs of the array and components can be optimized to achieve maximum array efficiency and to minimize the losses. The breadboard of a partial tent array is in the fabrication process. The performance of the components and array will be carefully evaluated to derive an achievable 30dB gain tent array design.

5.0 THE BREADBOARD ARRAY

A 4 x 6 breadboard array will be built and tested to demonstrate the feasibility of the tent array design. The array consists of 24 square

TABLE 6. THE DESIGN OF A TYPICAL 30dB GAIN TENT ARRAY

	Side Array	End Array	Total Array
Scan Sector	$\pm 63^{o}$	$\pm 30^{o}$	-
Tilt Angle	45^{o}	20^{o}	-
Minimum Coverage Gain (dB)	30	30	30
Total Losses (dB)	7.18	4.18	-
Directivity (dB)	37.18	34.18	-
Required Aperture Size (in^2)	1099	551	-
Element Spacing (in)	.78	.933	-
Array Depth - d (in)	6	7	-
Array Height - h' (in)	10.92	10.26	-
Array Width - w (in)	100.62	54.1	-
Array Elements	14 x 129	11 x 58	-
Number of Elements	1806	638	4888
Overall Array Size:			
Height - h (in)	12	12	12
Length - (in)	-	-	119
Radome Configuration			Modified 1E*

*See Figure 10.

waveguide elements including the septum polarizer, 24 3-bit diode phase shifters, a unique feed network, and a microprocessor. The array will be tested in the receive mode with the transmit port properly loaded. The objective of the breadboard is to demonstrate the performance of the critical components and to verify the concept of the tent shaped phased array. The array will be electronically scanned and antenna pattern characteristics will be measured. Then the performance of a 20dB gain full tent array will be induced. The results will also be extended to the 30dB gain tent array.

6.0 CONCLUSION

The tent shaped phase array provides fully electronic scanning and hemispherical coverage, and offers the potential for a lightweight, low-drag SHF aircraft antenna for satellite communications. A 20dB gain tent shaped array capable of handling high transmit power was designed to derive the optimum tent array configuration. The major design parameters include antenna gain, hemispherical coverage, aerodynamic impact, power handling capability, and array packaging. The array projected area plays a more important role than the radome streamline shape in the increase of fuel consumption percentage for the tent array requirements. The array depth has a significant impact on the aerodynamic effects and array packaging. The development and design of compact array components to reduce the array depth and to provide high power capability is the key factor to the successful application of the tent array concept.

The array configuration of the 20dB gain antenna was applied to the design of a 30dB gain antenna. The array depth has a less degree of impact on the aerodynamic effects and array packaging due to the fact that the antenna aperture of the end array dominates the projected area in the streamline direction. The array configuration and the design of components can be further optimized to achieve maximum array efficiency and to minimize the array loss.

Efforts will be concentrated on the hardware fabrication and measurement of the breadboard array for the remainder of the program. The measured antenna pattern characteristics will be analyzed to predict the performance

of a full-sized array and to ultimately verify the concept of the tent antenna.

REFERENCES

(1) Maune, J.J., "An SHF Airborne Receiving Antenna", 22nd Annual Symposium on USAF Antenna Research and Development, 1972.

(2) Mailloux, R.J., "Phased Array Aircraft Antennas for Satellite Communications", Microwave Journal Vol. 20 (No. 10), pp. 38-42, October 1977.

(3) Mailloux, R.J. and Mavroides, W.G., Hemispherical Coverage of Four-Faced Aircraft Arrays, RADC-TR-79-176, May 1979.

(4) Hoerner's, S.F., Fluid Dynamic Drag, Section 8-4.

(5) Davis, D., Digiondomenico, O.J., and Kempie, J.A., "A New Type of Circularly Polarized Antenna Element", IEEE PGAP Symposium Digest, 1967, pp. 26-31.

(6) Sharp, E.D.. "A Triangular Arrangement of Planar-Array Elements that Reduces the Number Needed", IRE Trans. on Antenna and Propogation, March 1961, pp. 126-129.

APPENDIX A

EQUATIONS OF COORDINATE TRANSFORMATIONS OF TENT ARRAY SYSTEM

Scan Contour. The computation of the scan contours involves coordinate transformations from array coordinates to aircraft coordinates. The definition and relationship of the coordinates are shown in Figure A-1. It is assumed that the array is lying on the xy plane of the array coordinates (x, y, z) and the y' of the aircraft coordinates (x', y', z') is pointing toward the zenith. The array is rotated around the x axis by an angle α, relative to the x', y', z' system. An observation point P, with distance r away from the origin, can be represented in either of the coordinate systems as shown in the following.

$$x = r\sin\theta\cos\theta \tag{A-1}$$
$$y = r\sin\theta\sin\phi$$
$$z = r\cos\theta,$$

$$x' = r\sin\theta'\sin\phi' \tag{A-2}$$
$$y' = r\cos\theta'$$
$$z' = r\sin\theta'\cos\phi'$$

The relationship of the coordinates systems is given by

$$x' = x \tag{A-3}$$
$$y' = \cos\alpha y + \sin\alpha z$$
$$z' = -\sin\alpha y + \cos\alpha z$$

From Equation (A-2), the angles (θ', ϕ') can be computed as

$$\phi' = \tan^{-1}\frac{x'}{y'}$$
$$\theta' = \tan^{-1}\frac{\sqrt{(x')^2 + (z')^2}}{y'} \tag{A-4}$$

The scan contours are the peak obtainable gain for the array beam scanned to the indicated direction (θ', ϕ') in aircraft coordinates. For small scan angles, the scanning gain Ps of the array is related to the peak gain in the array normal direction and can be approximated by

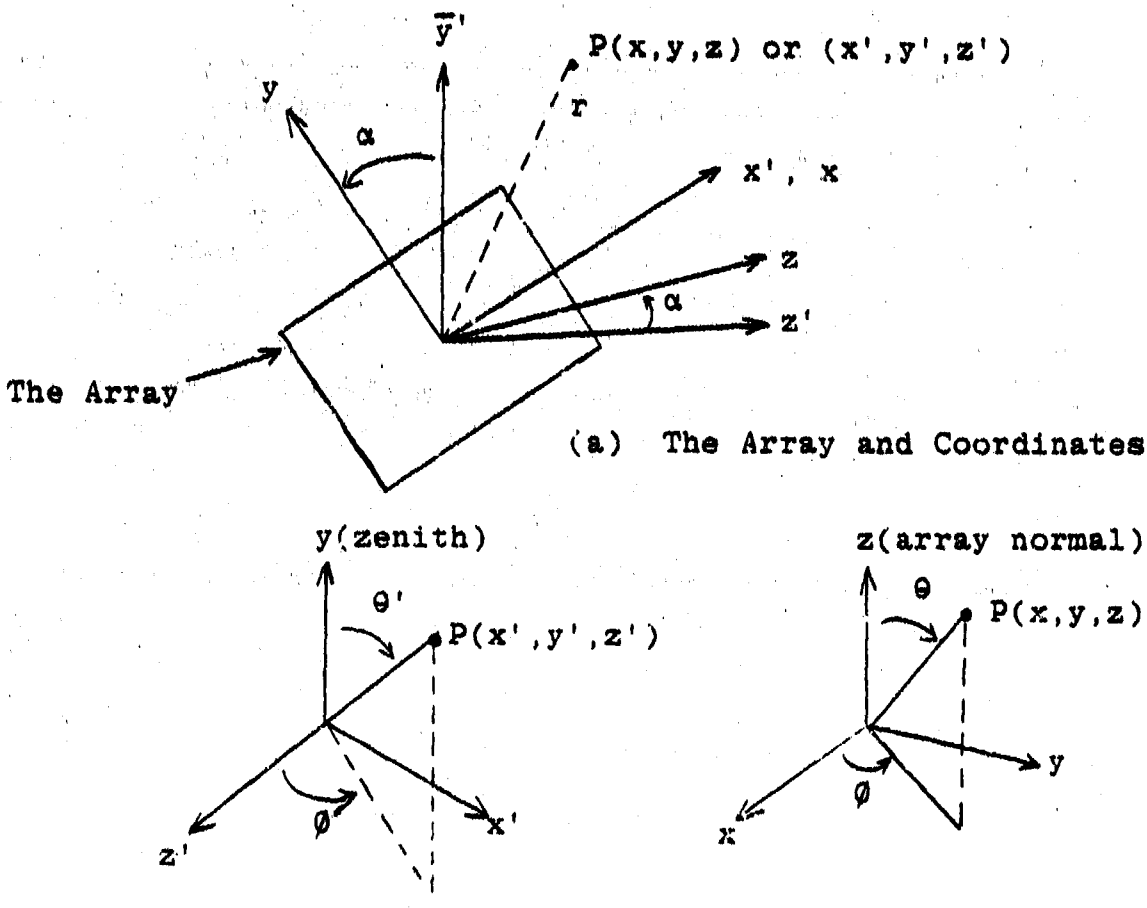

FIGURE A-1 AIRCRAFT AND ARRAY COORDINATES

$$Ps = \cos\theta, \qquad \text{for all } \phi \tag{A-5}$$

Ps is in general, directly related to the active element pattern which is a function of the isolated element pattern and mutual coupling effects of the array. It can be written:

$$Ps = f(\theta, \phi). \tag{A-6}$$

For a given scan gain level, the angles (θ, ϕ) are obtained using Equation (A-5) or (A-6), and the coordinates (θ', ϕ') can be computed using Equation (A-4).

Element Pattern. A given element pattern $\bar{E}$ in array coordinates can be represented by the element pattern $\bar{E}'$ in aircraft coordinates through the following transformation:

$$\bar{E}' = \begin{bmatrix} 0 \\ E\theta' \\ E\phi' \end{bmatrix} = uTS\,\bar{E} \tag{A-7}$$

where $\bar{E} = \begin{bmatrix} 0 \\ E\theta \\ E\phi \end{bmatrix}$

$$u = \begin{bmatrix} \sin\theta'\cos\phi' & \sin\theta'\sin\phi' & \cos\theta' \\ \cos\theta'\cos\phi' & \cos\theta'\sin\phi' & -\sin\theta' \\ -\sin\phi' & \cos\phi' & 0 \end{bmatrix}$$

$$T = \begin{bmatrix} 0 & -\sin\alpha & \cos\alpha \\ 1 & 0 & 0 \\ 0 & \cos\alpha & \sin\alpha \end{bmatrix}$$

$$S = \begin{bmatrix} \sin\theta\cos\phi & \cos\theta\cos\phi & -\sin\phi \\ \sin\theta\sin\phi & \cos\theta\sin\phi & \cos\phi \\ \cos\theta & -\sin\theta & 0 \end{bmatrix}$$

APPENDIX B
AN UNCONVENTIONAL SEPTUM POLARIZER

The waveguide and feed assembly of the side-facing array must either be loaded with dielectric material or the ridged waveguide used in order to prevent frequency cut off at low band due to the small element spacing at the array aperture. An alternative method is to use an unconventional septum in the polarizer region such to eliminate the use of dielectric material or ridged waveguide in this electrically sensitive region.

The concept of an unconventional septum polarizer treats the septum region as a combination of successive ridged waveguide sections and varies the waveguide dimension as the polarizer septum increases its depth toward the feeding structure. For a typical $\lambda o/2$ spaced square waveguide array, the main body of the unconventional septum polarizer is incorporated into a waveguide transition region where the square waveguide is doubly tapered into a rectangular waveguide of dimension λo by $\lambda o/4$ as shown in Figure B-1. The cross-sections and the dimensions of the polarizer element are given in Figure B-2.

A conventional septum polarizer maintains uniform waveguide inside dimensions so that the propagation constant, β, is constant for the field perpendicular to the septum and is a function of dimension b. The orthogonal mode generated by the septum, however, has a varying β', different from β. One explanation of how the polarizer works is that the differential phase between the two orthogonal modes can be made equal to $\frac{\pi}{2}$ due to the different propagation constants. Hence, it is assumed that the condition of

$$\int_0^L \beta'(l)dl - \beta L = \frac{\pi}{2} \quad ,$$

can be met to produce a circular polarization at the aperture.

In the proposed unconventional septum polarizer, the same phase difference for producing circular polarization is obtained by maintaining

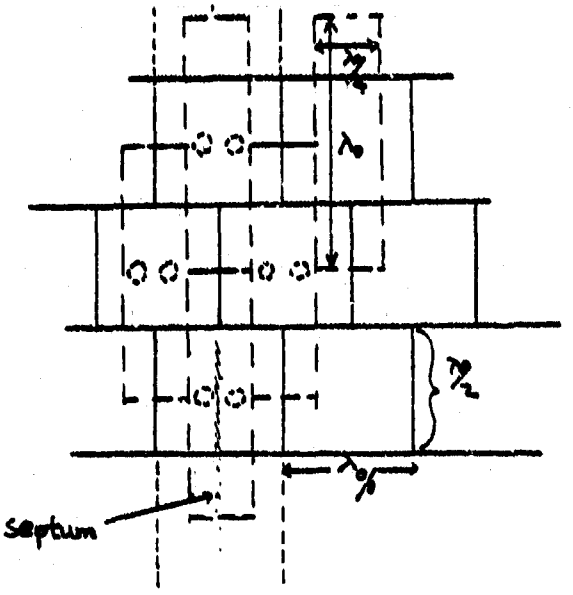

FIGURE B-1 STACKED UNCONVENTIONAL SEPTUMS

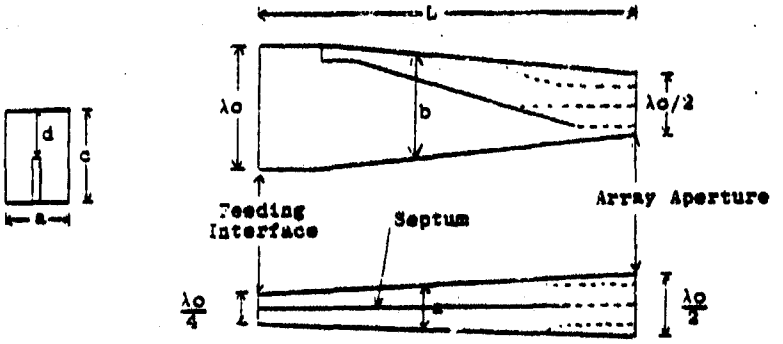

FIGURE B-2 CROSS SECTIONS OF THE UNCONVENTIONAL SEPTUM POLARIZER ELEMENT

β' constant and above cut-off. This is achieved by varying the septum dimension as the waveguide dimension a changes along the length. Using Pyle's* tables for single ridge waveguides and treating the septum region as a section of ridge waveguides, Table B-1 shows the waveguide dimensions in septum direction and the propagation constants β' of the sections.

Increment	a	$\lambda c/a$	$\lambda o/\lambda c$	β'	d/b
1	$0.5\lambda o$	2.4	.833	$3.476/\lambda o$	.60
.	.	.	.	.	.
.	.	.	.	.	.
11/2	$0.375\lambda o$	3.2	.833	$3.476/\lambda o$	.35
.	.	.	.	.	.
.	.	.	.	.	.
n	$0.25\lambda o$	4.8	.833	$3.476/\lambda o$	.15

TABLE B-1. WAVEGUIDE DIMENSIONS AND β'

In the above table, the values for β' are given by

$$\beta' = \sqrt{K^2 - Kc^2} = \sqrt{\left(\frac{2\pi}{\lambda o}\right)^2 - \left(\frac{2\pi}{\lambda c}\right)^2} = \frac{2\pi}{\lambda o}\sqrt{1 - \left(\frac{\lambda o}{\lambda c}\right)^2}$$

and is constant for constant value $\frac{\lambda o}{\lambda c}$. This is chosen as .833 which is a typical figure for the conventional septum polarizer. It can be seen from the table that the beginning dimension of the septum as .40b and the ending dimension of .85b are physically realizable. At the beginning, this dimension can be smoothly transformed to a ridge at the aperture (if the ridge is used at the element aperture); and at the end, the septum can join the opposite wall of the waveguide in a controlled notch (for impedance matching) to seal off the two input ports.

*J. R. Pyle; The cutoff Wavelength of the TE_{10} Mode in Ridged Rectangular Waveguide of Any Aspect Ratio; IEEE Transactions of Microwave Theory and Techniques, April 1966.

The propagation constant β for the field perpendicular to the septum in this case will be varying since the dimension b is varying. The following table lists a few of the values along the element.

b	$\lambda c/b$	$\lambda o/\lambda c$	β
$0.6\lambda o$	2	.833	$3.476/\lambda o$
$0.9\lambda o$	2	.556	$5.222/\lambda o$
$1.0\lambda o$	2	.417	$5.711/\lambda o$

TABLE B-2. WAVEGUIDE DIMENSIONS AND β

It is seen from this table that β will get larger and larger as b gets wider. However, for the part of the transition near the aperture where $0.5\lambda o \leq b < 0.6\lambda o$, there will be a need for an extension of the aperture ridges to keep $\frac{\lambda o}{\lambda c}$ less than .833.

Then the cumulative effects can be made such that:

$$\int_0^L \beta(l)dl - \beta' L = \pi/2$$

which is the opposite of the case for the conventional septum polarizer. However, it should be noted that this polarizer will be polarized in the opposite sense compared with the conventional one.

APPENDIX C

THE COMPUTATION OF ELEMENT PATTERN OF THE TENT ARRAY

The active element pattern of the tent array can be estimated using infinite array theory, and the fuselage ground plane effects on the element pattern can be computed employing the theory of geometrical optics. The fuselage of the aircraft is approximated by a conducting circular cylinder of radius a. The array is located on the xy plane of the array coordinate system (x, y, z) which is tilted around the x-axis by angle α in relation to the aircraft coordinate system (x', y', z'). The array and the cylindrical ground plane are shown in Figure C-1. The equations following describe the radiation fields of the element pattern in the plane normal to the cylinder and in other directions.

The total radiation field from Source 0 (the phase center of the element of interest) at observation point P can be written as

$$\bar{E} = \bar{E}^i(P)u^i + \bar{E}^r u^r \qquad (C\text{-}1)$$

in which $\bar{E}^i$ is the electrical field of the active element pattern of the source in the absence of the surface, $\bar{E}^r$ is the reflected field from the point θ_R can be found using Snell's law at the cylindrical surface. The functions u^i and u^r are unit step functions which are equal to one in the illumination regions and to zero in the shadow regions. The active element pattern $\bar{E}^i$ can be represented by*

$$\bar{E}^i(r) = \frac{(k^2 st \sin\Omega \sin 2\theta)}{4\pi} \left[-\bar{T}(\theta,\emptyset)\bar{\theta} + T(\theta,\emptyset)\bar{\emptyset}\right] \frac{e^{-jkr}}{r} \qquad (C\text{-}2)$$

where k is the wave number, s, t, are dimensions and Ω is the angle of the arrayarray lattice as shown in Figure C-2, $\bar{\theta}$, $\bar{\emptyset}$ are spherical coordinates of the array coordinate system. $\bar{T}$ and T are the mainbeam transmission coefficients of the cophasal array in which all of the elements are excited with equal magnitude and a progressive phase such that the mainbeam is pointed to the direction $(\theta,\emptyset)$.

*C. A. Chuang & S. W. Lee, "Active Element Pattern of a Rectangular Wave-Guide in a Periodic Planar Array", a976 URSI Digest, Oct. 10-15, 1976, Amherst, Massachusetts.

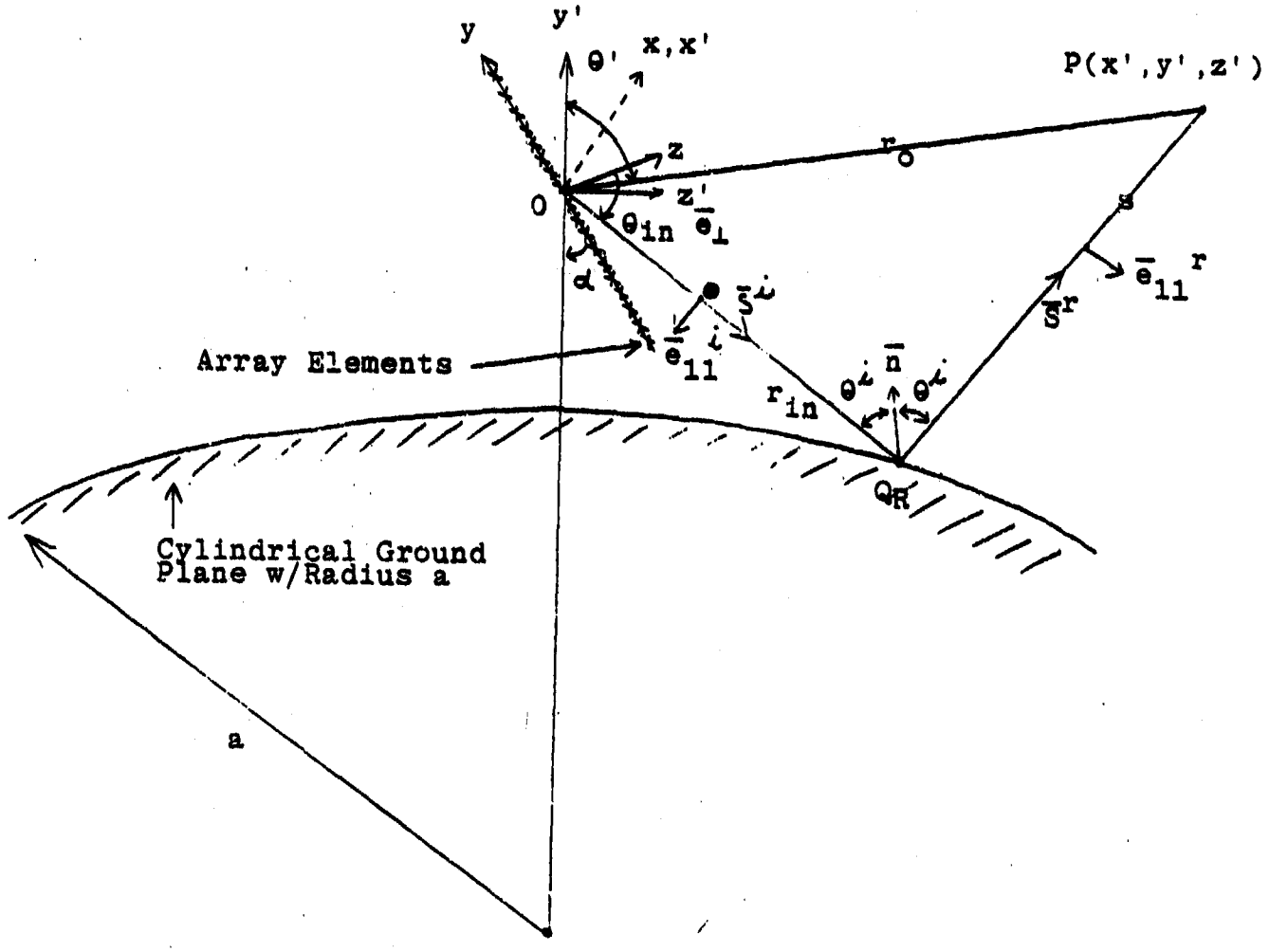

FIGURE C-1 ARRAY AND THE CYLINDRICAL GROUND PLANE

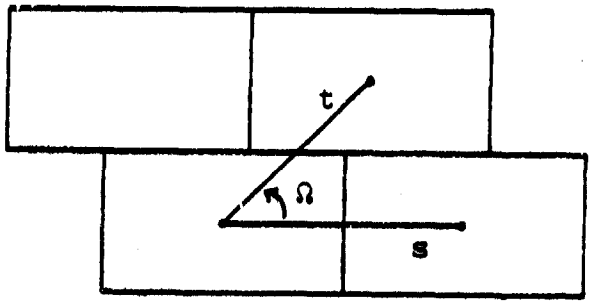

FIGURE C-2 ARRAY ELEMENTS AND GRIDS

The reflected field $\bar{E}^r$ can be written** as

$$\bar{E}^r(s) = \bar{E}^i(\theta_R)\cdot\bar{R}\sqrt{\frac{P_1^r P_2^r}{(P_1^r + s)(P_2^r + s)}}\, e^{-jks} \qquad (C\text{-}3)$$

in which P_1^r, P_2^r are the principal radii of curvature of the reflected wavefront at the point of reflection θ_R, and s is the distance from θ_R to the observation point P(x', y', z').

The dyadic reflection coefficient matrix $\bar{R}$ is given by

$$\bar{R} = \left[\bar{e}_{11}{}^i\bar{e}_{11}{}^r - \bar{e}_\perp\bar{e}_\perp\right] \qquad (C\text{-}4)$$

with $\bar{e}_\perp$ the unit vector perpendicular to the incident ray, and $\bar{e}_{11}{}^r$, $\bar{e}_{11}{}^i$, the unit vectors parallel to the plane of incidence as shown in Figure C-1.

The incident field $\bar{E}^i(\theta_R)$ at reflection point θ_R can be written as

$$\bar{E}^i(\theta_R) = (A\bar{e}_{11}{}^i + B\bar{e}_\perp) \qquad (C\text{-}5)$$

in which $C = \frac{k^2 st \sin\Omega \sin\theta in}{4\pi}\ \frac{e^{-jkr_{in}}}{r_{in}}$, A, B are functions of $\bar{T}$, T, obtained through the coordinate transformation (from $\bar{\theta}$, $\bar{\emptyset}$ to $\bar{e}_{11}{}^i$, $\bar{e}_\perp$), and r_{in} is the distance from the source to θ_R.

The principal radii of curvature of the reflecting surface has been derived by Kouyoumjian** in ray coordinates and are given by

$$\frac{1}{P_1{}^r} = \frac{1}{r_{in}} + \frac{2\sin^2\theta_2}{a\cos\theta^i} \qquad (C\text{-}7)$$

and

$$\frac{1}{P_2{}^r} = \frac{1}{r_{in}}$$

**R. G. Kouyoumjian and P. H. Pathak, "A Uniform Geometrical Theory of Diffraction for an Edge in a Perfectly Conducting Surface", Proc. of IEEE, November 1974, pp. 1448-1461.

in which θ^i is theincident angle in reference to the surface normal $\bar{n}$ at θ_R, and θ_2 is the angle between the incident ray $\bar{s}^i$ and principal direction $\bar{x}$ (axial direction) of the cylindrical surface at θ_R.

It should be noted that $\bar{E}^r$ in Equation C-3 is expressed in coordinates ($\bar{e}_{11}{}^r$, $\bar{e}_{\perp}$). It can be transformed to coordinate ($\bar{\theta}$,$\bar{\phi}$) and be added with $\bar{E}^i$ in Equation C-2 to obtain the total field at point P.

MISSION
of
Rome Air Development Center

RADC plcns and executes research, development, test and selected acquisition programs in support of Command, Control Communications and Intelligence (C^3I) activities. Technical and engineering support within areas of technical competence is provided to ESD Program Offices (POs) and other ESD elements. The principal technical mission areas are communications, electromagnetic guidance and control, surveillance of ground and aerospace objects, intelligence data collection and handling, information system technology, ionospheric propagation, solid state sciences, microwave physics and electronic reliability, maintainability and compatibility.

Printed by
United States Air Force
Hanscom AFB, Mass. 01731